Applied Energy 260 (2020) 114314

Contents lists available at ScienceDirect

Applied Energy

journal homepage: www.elsevier.com/locate/apenergy

An integrated tool for optimal energy scheduling and power quality improvement of a microgrid under multiple demand response schemes

Dimitrios Thomas[a,b,*], Gaspard D'Hoop[a], Olivier Deblecker[a], Konstantinos N. Genikomsakis[b], Christos S. Ioakimidis[b]

[a] Department of Electrical Engineering, University of Mons, 7000 Bd Dolez 31, Mons, Belgium
[b] ERA Chair 'Net-Zero Energy Efficiency on City Districts', Research Institute for Energy, 7000 Rue de l'Epargne 56, Mons, Belgium

HIGHLIGHTS

- Energy scheduling for optimal power dispatch and total system cost minimization.
- Financially incentivized flexibility services between microgrid and market operator.
- Framework which checks and mitigates power quality issues of the optimal solution.
- Power quality restored with a small number of iterations and additional system cost.

ARTICLE INFO

Keywords:
Buildings-to-grid integration
Energy management system
Harmonic distortion
Optimization
Power quality
Smart grid

ABSTRACT

This paper presents an integrated tool to mitigate power quality issues in a microgrid through coordinating the operating schedule of its generating resources and loads. Such a microgrid includes renewable and conventional distributed energy resources, electric vehicles, energy storage, linear and nonlinear loads, while it serves as an example small-to-medium scale residential and commercial buildings. The proposed tool operates on a sequential, two-stage basis: at the first stage the energy management system (EMS) ensures that the microgrid's generation resources and loads are dispatched at the minimum total system cost. In addition, it assesses the potential provision of flexibility services towards the system operator, relying on financially incentivized power signal requests. At the second stage, the power quality (PQ) framework evaluates whether the proposed optimal solution complies or not with several PQ standards applicable to the distribution level. The unique characteristic of the proposed tool is the self-triggered interaction between the EMS and the PQ framework, which identifies potential PQ violations, and restores the PQ indices to acceptable levels through an iterative process. Case studies have been performed with realistic model parameters to verify the performance of the proposed integrated tool. The obtained results demonstrate the effectiveness of the algorithm in managing voltage deviations, voltage unbalance, as well as harmonic distortions with a small additional cost for the total system.

1. Introduction

1.1. Background and motivation

A microgrid is a low-voltage power distribution system organized based on the control capabilities over the main network and it is characterized by distributed energy resources (DERs) and controllable loads. DERs comprise a variety of distributed generation (DG) units such as photovoltaics (PVs), distributed storage units (batteries, energy capacitors, etc.), wind turbines, and autonomous power stations (APS) which usually consume diesel or heavy oil (mazut) fuel. Controllable loads such as electric vehicles (EVs), heating, ventilation, and air-conditioning (HVAC) systems can be deferred or shed to balance supply and demand in the microgrid. Power flow in microgrids is controlled and monitored by an energy management system (EMS) ensuring that specific operational objectives (e.g., cost minimization) are met. To achieve this, an EMS adjusts the power imported from or exported to the main grid, the operation and dispatch of DERs, and the controllable loads [1].

Microgrids propose new features to electricity industry offering additional possibilities for multi-stage electrical power grid operation, control and management. Some of the new features comprise advanced

* Corresponding author.
E-mail address: dimitrios.thomas@umons.ac.be (D. Thomas).

https://doi.org/10.1016/j.apenergy.2019.114314
Received 10 July 2019; Received in revised form 29 November 2019; Accepted 1 December 2019

Nomenclature

$\alpha_{l,t}^{\Delta V,\text{lim}}$	parameter bounding $\alpha_{l,t}^{\Delta V}$ at each iteration
$\alpha_{l,t}^{\Delta V}$	artificial variable for restoring voltage deviation index
$\alpha_t^{\text{hd,lim}}$	parameter for bounding $\alpha_t^{\text{hd,lim}}$ at each iteration
α_t^{hd}	artificial variable for restoring voltage harmonic distortion index
$\alpha_t^{\text{unb,lim}}$	parameter for bounding $\alpha_t^{\text{unb,Ph}(\cdot)}$ at each iteration
$\alpha_t^{\text{unb,Ph}(\cdot)}$	artificial variable for restoring voltage unbalance index
λ^{hd}	sensitivity parameter related with the rate of change of α_t^{hd}
λ^{unb}	sensitivity parameter related with the rate of change of $\alpha_t^{\text{unb,Ph}(\cdot)}$
$\lambda_{\Delta V}$	sensitivity parameter related with the rate of change of $\alpha_{l,t}^{\Delta V}$
$\widetilde{\varepsilon}$	value of residual energy [$/kWh]
$\varepsilon_t^{\text{buy/sell}}$	day ahead electricity buy/sell price at time t [$/kWh]
$\xi_{(\cdot),t}$	auxiliary binary variable
$C^{\text{grid,react.}}$	penalty factor to restrict the reaactive power exhange with the grid [$/kVAR]
$C^{\text{EV,deg}}$	EV battery degradation cost [$/kWh]
$C^{\text{DER,react.}}$	penalty factor to restrict the reaactive power exhange among microgrid DERs [$/kVAR]
$C_r^{\text{DG,op}}$	operational cost for DG r [$/kWh]
C_r^{ST}	start-up cost for DG r [$]
$L_t^{\text{dem}(\cdot)}$	limit of demand-related active power alteration request at time t [kW]
$L_t^{\text{sup}(\cdot)}$	limit of supply-related active power alteration request at time t [kW]
$p_{k,t}^{\text{EV,ch/dis}}$	(dis) charging power of EV k at time t [kW]
$p_{l,ty,t}^{\text{load}}$	active power to serve load l of type ty at time t [kW]
$p_{r,t}^{\text{DG}}$	active power from DG r at time t [kW]
$p_{s,t}^{\text{ES,dis/ch}}$	(dis) charging power of storage s at time t [kW]
$p_t^{\text{grid,in/out}}$	active power drawn from/ injected to the grid at time t [kW]
$q_{l,ty,t}^{\text{load}}$	reactive power to serve load l of type ty at time t [kVAR]
$q_{s,t}^{\text{ES,gen/abs}}$	reactive power generated/absorbed from storage s at time t [kVAR]
$q_{r,t}^{\text{DG,gen/abs}}$	reactive power generated/absorbed from DG r at time t [kVAR]
$q_t^{\text{grid,in/out}}$	reactive power drawn from/ injected to the grid at time t [kVAR]
$R_t^{\text{dem}(\cdot)}$	reward for meeting demand-related request at time t [$/kWh]
$R_t^{\text{sup}(\cdot)}$	reward for meeting supply-related request at time t [$/kWh]
$soe_{k,t}^{\text{EV}}$	state of energy for EV k at time t [kWh]
$soe_{s,t}^{\text{ES}}$	state of energy for storage s at time t [kWh]
$z_t^{\text{dem}(\cdot)}$	total active power demand related with demand request alteration [kW]
$z_t^{\text{sup}(\cdot)}$	total active power supply related with supply request alteration [kW]

Acronyms

APS	Autonomous Power Station
DA	Day Ahead
DER	Distributed Energy Resource
DG	Distributed Generation
DHW	Domestic Hot Water
DR	Demand Response
DSO	Distribution System Operator
EMS	Energy Management System
ES	Energy Storage
EV	Electric Vehicle
HVAC	Heating Ventilation Air-Conditioning
IEEE	Institute of Electrical and Electronics Engineers
MILP	Mixed Integer Linear Programming
PCC	Point of Common Coupling
PF	Power Factor
PQ	Power Quality
PV	Photovoltaic
RMS	Root Mean Square
TC	Total Cost
THD	Total Harmonic Distortion
VOLL	Value of Lost Load
VUF	Voltage Unbalance Factor
WT	Wind Turbine
X/R	Reactance on Resistance ratio

smart metering, demand-side management systems and communication infrastructure providing real-time information for all system variables [2]. On the one hand and from a microgrid's point of view the aforementioned features combined with a demand-response (DR) strategy can decrease the total cost of energy supply, meeting at the same time microgrid's electricity and thermal demands. On the other hand, a microgrid can provide flexibility to a distribution system operator (DSO) in the form of ancillary services by responding to its signals for power supply/demand increase/decrease [3]. In addition, the accelerated development of microgrid has paved the way for the interconnection of multiple microgrids to provide regional power supply. As a result, the power exchange and the coordination of the DG units within the individual microgrids forming a multi-microgrid system is a complex problem that requires efficient and reliable energy management [4].

An important advantage of microgrids lies on their ability to remain operational even when the public power network encounters extensive blackouts. By taking advantage of their on-site distribution generation, microgrids can supply critical loads and keep crucial consumers in operation during blackouts in islanded mode. However, despite the aforementioned essential advantage, several reasons may prevent the uninterrupted and smooth islanded microgrid operation. The most frequent and significant reasons are: DG may not be able to regulate the voltage and frequency within the islanded system, fault contribution from DG may not be sufficient to allow satisfactory operation of protection systems, the parallel operation of DG units within the islanded mode may cause problems, etc. [5]. Therefore, it is important to determine the requirements for a safe and reliable microgrid operation which is able to overcome the above-mentioned challenges. Such an energy management framework which combines proactive and reactive approaches to efficiently address the uncertainties associated with generation and demand in islanded and interconnected microgrids is proposed in [6].

One of the primary operational challenges that arises in a microgrid, either it is related with its own EMS operation (in grid-connected or islanded mode), or with its action as an ancillary service to the DSO, is associated with power quality (PQ) management. Due to the usually small generation capacity, the physical operating characteristics of the microgrid's equipment and appliances can substantially affect the microgrid current, voltage and frequency resulting in harmful harmonic distortions. Thus, the microgrid's equipment operating characteristics must be sufficiently modeled taking into count both the fast time scales related with local controls and the longer time scales associated with energy scheduling.

This paper proposes an integrated tool for the cooperative evaluation of optimal EMS operation in a microgrid combined with a concurrent power quality assessment. The mixed integer linear programming (MILP) energy scheduling algorithm decides the DERs optimal dispatch based on a given operational objective meeting microgrid's load requirements. At the same time, microgrid power quality is monitored to ensure it complies with IEEE standards for distribution networks. A potential violation in any of these standards triggers the initiation of an iterative algorithm which restores the microgrid's power quality indices back to acceptable values.

The primary motivation for this paper is the recent development in building technologies, such as intelligent automated systems, which can enhance EMS control technologies and operation to achieve improved economic and operational objectives.

1.2. Related work and contributions

Several studies in literature propose energy scheduling algorithms for optimizing specific objectives under EMS operation in microgrids/smartgrids. Özkan [7] introduces a home power management system with a corresponding rule-based control algorithm over smart electric appliances to reduce total cost and lower peak demand. The authors in [8] use neural networks to develop a DR control system in residential sector implementing PV and electricity storage. Xue et al. [9] introduce an interactive DR strategy which focuses on commercial buildings integrating renewable energy. Chen et al. [10] implement stochastic and robust optimization to evaluate the real-time price-based DR management for residential appliances. Monte Carlo simulation is used for minimizing the expected electricity payment, while price uncertainty intervals are used in the robust optimization for minimizing the worst-case electricity payment. Adopting a two-frame algorithm, Bendato et al. [11] propose an EMS to integrate economical aspects and system operator requirements using among others forecasting data analysis. During the first step, the optimal active power of the microgrid's DGs is calculated minimizing the total production cost, while in the second step the reactive power of the programmable units is decided to meet the system operator requirements.

The consideration of EVs as a reliable alternative DER, among others, is reflected in the increasing number of studies tackling their integration in microgrids. Existing works cover a broad range of EVs applications such as bidirectional energy trading capabilities [12], optimal scheduling for EVs charging/discharging [13], impact on the grid [14,15], peak shaving and load shifting [16] and utilization of EVs as alternative storage potential [17]. As the electric vehicle deployment is growing worldwide, their proper integration in electricity grids becomes more and more important.

Meanwhile, several studies have been conducted applying the multi-objective approach for EMS/DR operation [18]. The optimal solutions are known as Pareto-optimal solutions and offer the best trade-offs among all the defined and conflicting objectives. The authors in [19] propose a MILP model to schedule the energy consumption within smart homes in a microgrid. The two conflicting objectives are to minimize the daily energy cost and CO_2 emissions. Coelho et al. [20] describe a multi-objective power dispatching problem that uses EVs as storage units optimizing several objectives like total costs, EVs batteries usage, and maximum peak load. The authors in [21] present a multi-objective generation scheduling model for pricing demand response rate in micro-grid energy management optimizing operation cost and emissions, while the authors in [22] propose a DR management framework which minimizes both the cost of energy production and the discomfort of community-based microgrid.

From another point of view, a series of studies in the literature focus mainly on addressing power quality issues in a microgrid, such as voltage instability and unbalance [23], harmonic distortion, frequency variations, etc., without taking into account whether the conducted power transient analysis corresponds to microgrid's optimal operation from the scope of the selected operational objective. The authors in [24] propose a "Smart Branch" for microgrids power quality improvement by implementing a finite control set-model predictive controller which tracks pure sinusoidal wave forms as its references. Adnan et al. [25] use probabilistic modeling to formulate the complexity of randomness for load flow balancing through a smart node and transient stability analysis through a unified power flow controller, while many studies focus on assessing power quality characteristics of photovoltaic systems and EVs with respect to the grid [26,27]. Moreover, the impact of harmonic distortion on microgrid's power quality has been also addressed systematically in the literature [28,29].

The papers referred in this study have provided respective contributions to the application of energy management systems and power scheduling algorithms. However, research has tended to focus either on operational objectives, such as optimal DERs dispatch (EMS and DR development), or on power quality analysis (voltage/current deviations, harmonic disorders, etc.) of a microgrid. This paper proposes an integrated tool which, on the one hand, implements a MILP model to optimally decide the operation of an EMS using several DERs to minimize total system cost, and on the other hand, additionally applies power flow and total harmonic distortion analysis in the microgrid to identify power quality-related operational issues and adjust their values in compliance with IEEE standards, when necessary. The unique contributions of this paper, in the form of an integrated tool, are therefore:

- A bidirectional MILP-based energy scheduling algorithm to minimize total system cost in a microgrid implementing DERs such as APS, PV, wind turbines, EVs, and storage.
- A binary-based power exchange framework (incorporated in the EMS algorithm) to model the potential interaction between the microgrid and the DSO. The framework operates on the basis of financially incentivized power signal requests.
- A self-triggered, iterative algorithm which monitors the microgrid power quality and intervenes to restore the corresponding indices to acceptable levels when a violation in standards is identified.

To the best knowledge of authors, the present study is original in incorporating the previously mentioned characteristics in a single integrated tool. The proposed integrated tool is evaluated under several energy schemes and operational scenarios within the microgrid such as rapid load increase/decrease, sudden power cuts leading to off-grid standalone operation, abrupt voltage phase unbalance, etc.

1.3. Organization

In the remaining paper, Section 2 describes the general structure of the proposed integrated tool and reviews the assumptions and limitations. Section 3 provides the mathematical formulation of the energy scheduling algorithm, while Section 4 identifies the power quality issues in microgrid operation and presents the mathematical formulation of the power quality framework. Section 5 introduces the microgrid model used in the simulations and it illustrates a number of case studies where the operation and effectiveness of the proposed energy management integrated tool is demonstrated. Finally, Section 6 draws the conclusion of this paper and suggests future work.

2. General structure of the proposed integrated tool

2.1. Interaction of EMS and PQ framework

The proposed integrated tool consists of an EMS and a PQ framework which operate on a sequential basis. During the first step, the EMS decides the optimal energy schedule of all the distributed energy resources, the distributed generation units and the loads based on a specific operational objective (total system cost minimization) for a period of 24 h in day-ahead. More specifically, it calculates:

- the active/reactive power of the DERs/DGs;
- the active/reactive power that the microgrid exchanges with the electricity grid;
- the extent the loads are met (taking into consideration the value of lost load).

The necessary input data for the EMS include among others: the renewable energy DA forecasts, the DA electricity price, the microgrid loads, the initial state of charge and the arrival/departure schedule of the EVs, the charge/discharge rates for both the EVs and the storage system, etc. The EMS is implemented in GAMS [30] and is solved with the CPLEX 12.7 solver. The mathematical formulation of the EMS is provided in Section 3.

The PQ framework is activated at the second step of the proposed integrated tool. All the calculations related with the PQ analysis and check, occur during this step (power flow and harmonics analyses). To assess the PQ of the microgrid, three different indices are introduced: the voltage variation, the total harmonic distortion (THD), and the voltage unbalance factor (VUF). These PQ indices are checked for every hourly time frame. A potential violation of the standards that have been set for each one of the PQ indices initiates the PQ improvement iterative process and activates the PQ constraints. This is a process that coordinates the interaction between the EMS and PQ framework to restore the PQ indices to acceptable values. The power flow, the network steady state harmonic analysis, as well as the PQ indices described above are programmed and calculated using MATLAB [31] and OpenDSS [32]. A more detailed description on the PQ framework is given in Section 4.

The flowchart in Fig. 1 illustrates the operation of the proposed integrated tool. First, the optimal energy schedule solution is obtained from the EMS without any power quality check. The acquired microgrid active/reactive power schedule is the input of the power quality framework. After the power flow and harmonics analyses, the initial energy schedules of both loads and generation resources are evaluated for voltage variation, harmonic distortion, and phase unbalance using OpenDSS. If any violations against the power quality standards are detected, energy scheduling is solved again, enforcing this time the PQ constraints. The iteration continues until all power quality indices are controlled under requirement levels.

2.2. Assumptions and limitations

We now review some general assumptions and limitations about the proposed integrated tool. First, we assume that the wind and solar generation data (as these are provided in [33]) reflect accurate DA forecasts. Moreover, although in reality retail electricity rates tend to be regulated, different across the types of distribution customers, and varying depending on the utility provider, for the sake of simplicity we assume the same DA electricity rate across all microgrid's generation resources and loads. It is also assumed that the EVs fleet is homogenous, namely that it is composed of the same type of vehicle with the same battery capacity and charging/discharging efficiency. The homogenous EVs fleet is selected for simplicity reasons. Although a heterogeneous fleet of EVs would be closer to reality, it would not differentiate the operation of the proposed algorithm for charging/discharging the EVs fleet. In addition, the EVs schedule corresponds to work-related trips which affects their arrival/departure times to and from the microgrid.

As far as the limitations are concerned, one should notice that the proposed integrated tool operates as an assessment tool in DA. It focuses on evaluating different energy demand response scenarios and the power quality anomalies that these scenarios may cause. However, the proposed tool is not recommended to assess real-time situations, as the hourly time-frame that has been selected for the simulations is not suitable for responding to transient changes of state. Moreover, as the optimization horizon is relatively short (one day), investment and maintenance costs associated with the microgrid's operation are not taken into consideration.

3. The EMS scheduling algorithm

In this section, we provide the mathematical formulation for the EMS algorithm. We also discuss the operation of DERs and the nature of loads in more detail. One should notice that discrete energy management policies can lead to different scheduling and EMS strategies in

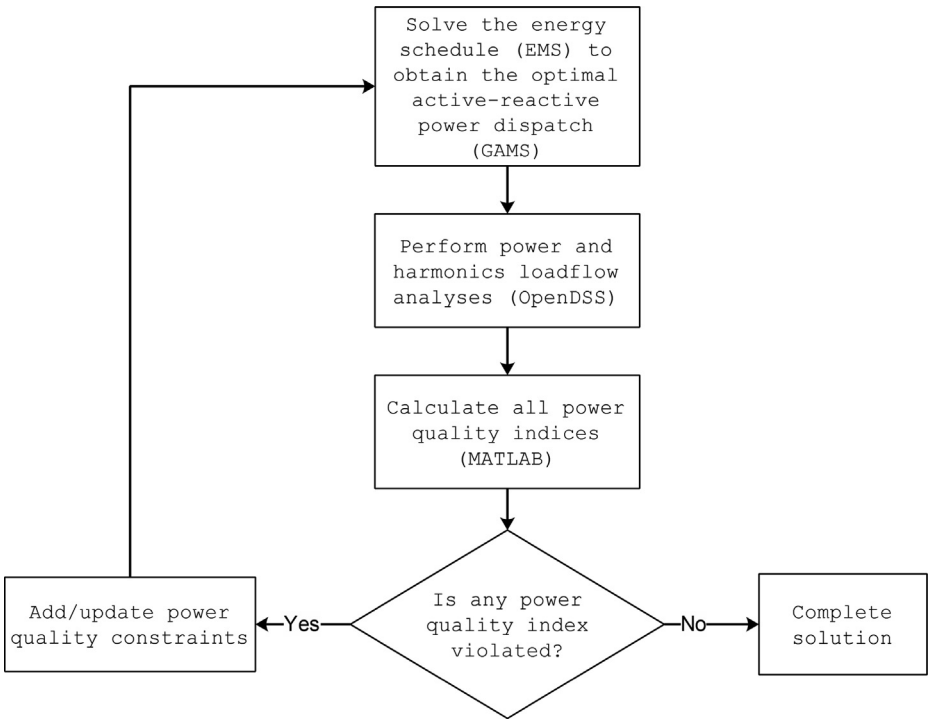

Fig. 1. Energy scheduling and power quality check of the proposed integrated tool.

microgrids. For example, the microgrid operator and the microgrid stakeholders/occupants can belong to the same economic entity expressing common economic interests. In this case, energy scheduling focuses mainly on prioritizing appliance and equipment operations, while assuming realistic supply costs and VOLL. On the other hand, the microgrid operator and the microgrid stakeholders/occupants may belong to multiple economic entities with contradicting economic interests, like for example energy suppliers (could be the DERs owners) and consumers (expressed for instance by the loads). The EMS proposed in this paper has been formulated to operate under the former described energy policy. However, with slight modifications it should be able to support the latter policy, as well.

The microgrid operator performs day-ahead central energy scheduling. The algorithm determines the optimal dispatch and operation of the available supply resources (energy from the grid, DERs, EVs) and load equipment over the planning time horizon (one day divided in hourly time-steps) to minimize the total system cost. At the same time, all the physical operating requirements of the microgrid are taken into account, including the power quality requirements. The objective function which minimizes the total system cost over the study time horizon, is given by Eq. (1) below:

$$\begin{aligned}
\underset{\Xi}{\text{Minimize}} \sum_{r,t} \Big(& \underbrace{C_r^{\text{DG,op}}\, p_{r,t}^{\text{DG}}}_{\text{Operational DG cost}} + \underbrace{C_r^{\text{ST}}\, \xi_{r,t}^{\text{ST}}}_{\text{Start-up DG cost}} \Big) \\
& + \sum_{t} \underbrace{\left(p_t^{\text{grid,in}}\, \varepsilon_t^{\text{buy}} - p_t^{\text{grid,out}}\, \varepsilon_t^{\text{sell}}\right)}_{\text{Grid energy exchange}} \\
& + \sum_{l,ty,t} \underbrace{\left(p_{l,ty,t}^{\text{load,max}} - p_{l,ty,t}^{\text{load}}\right) VOLL_{ty}}_{\text{Value of lost load}} - \sum_{s} \underbrace{\widetilde{\varepsilon}\; soe_{s,T}^{\text{ES}}}_{\text{Residual ES energy}} \\
& - \sum_{t} \underbrace{\left(R_t^{\text{sup}\uparrow}\, z_t^{\text{sup}\uparrow} + R_t^{\text{sup}\downarrow}\, z_t^{\text{sup}\downarrow} + R_t^{\text{dem}\uparrow}\, z_t^{\text{dem}\uparrow} + R_t^{\text{dem}\downarrow}\, z_t^{\text{dem}\downarrow}\right)}_{\text{Revenue from meeting DSO requests}} \\
& + \sum_{k,t} \underbrace{\left(p_{k,t}^{\text{EV,ch}} + p_{k,t}^{\text{EV,dis}}\right) C^{\text{EV,deg}}}_{\text{Penalty for EV battery degradation}} + \sum_{t} \underbrace{\left(q_t^{\text{grid,in}} + q_t^{\text{grid,out}}\right) C^{\text{grid,react.}}}_{\text{Penalty for grid reactive power}} \\
& + \sum_{t} \underbrace{C^{\text{DER,react.}} \left[\sum_{s} \left(q_{s,t}^{\text{ES,gen}} + q_{s,t}^{\text{ES,abs}}\right) + \sum_{r} \left(q_{r,t}^{\text{DG,gen}} + q_{r,t}^{\text{DG,abs}}\right) \right]}_{\text{Penalty for reactive power exchange within the DERs in the microgrid}}
\end{aligned} \tag{1}$$

where Ξ is the set that contains all the primal optimization variables. One should notice that since the considered time step is one hour, power and energy values coincide.

The first term of Eq. (1) minimizes the operational $C_r^{\text{DG,op}}\, p_{r,t}^{\text{DG}}$ and the start-up $C_r^{\text{ST}}\, \xi_{r,t}^{\text{ST}}$ cost of the DGs, where $\xi_{r,t}^{\text{ST}}$ is an integer binary variable expressing whether a DG *r*starts to operate at time *t*or not. The set of the DGs comprises the two APS units, the PV unit, and the wind turbine. For the renewable DGs, we assume a negligible operational cost, while their start-up cost has been set to zero. The second term aims at minimizing the power $p_t^{\text{grid,in}}$ requested from the grid at price $\varepsilon_t^{\text{buy}}$, while at the same time maximizing the power $p_t^{\text{grid,out}}$ injected to the grid at price $\varepsilon_t^{\text{sell}}$. We consider the selling price $\varepsilon_t^{\text{sell}}$ to be 10% lower than the buying price $\varepsilon_t^{\text{buy}}$ [34]. The third term of Eq. (1) minimizes the cost subsequent to the shed load. Variable $p_{l,ty,t}^{\text{load,max}}$ expresses the anticipated load without any deferral or shed, while variable $p_{l,ty,t}^{\text{load}}$ is the actual load served. Their difference indicates the shed/lost load which is penalized by the VOLL.

The term $\widetilde{\varepsilon}\; soe_{s,T}^{\text{ES}}$ is the so-called *energy value* and reflects the value of each kWh of the residual energy in ES ($soe_{s,T}^{\text{ES}}$) at the end of the time horizon considered, i.e., $t = T$ [35]. Unlike more studies where residual energy at the end of the scheduling horizon is either kept equal to the initial state-of-charge or anchored within an acceptable deviation from initial level [36], the concept of energy value is used here to reflect the value of the residual energy in ES, as the residual energy has the potential to yield profits by generating (discharging) in the following horizons. Consequently, a price $\widetilde{\varepsilon}$ is assigned to the final energy level (state-of-energy) to reflect its value, and the resulting energy value is considered in the objective function.

The fifth term of the objective function characterizes a revenue for the microgrid, provided that it meets the DSO requests for an increase/decrease in microgrid's total power supply ($z_t^{\text{sup}\uparrow}$, $z_t^{\text{sup}\downarrow}$) to, or demand ($z_t^{\text{dem}\uparrow}$, $z_t^{\text{dem}\downarrow}$) from the main grid. The remaining terms of Eq. (1) constitute penalty factors to ensure microgrid's smooth operation. Specifically, the sixth term applies a small cost $C^{\text{EV,deg}}$, every time an EV charges ($p_{k,t}^{\text{EV,ch}}$) or discharges ($p_{k,t}^{\text{EV,dis}}$). This is to ensure that no unnecessary EV charges/discharges take place and to prevent EVs' battery degradation. The seventh and eighth terms impose a fictitious cost to limit the reactive power exchange, not only between the microgrid and the main grid, but also among the DERs and the DGs within the microgrid itself to avoid excessive power losses in the distribution cables. The operating constraints are described as follows.

3.1. Loads

To represent the diversity of loads present in the system, each aggregated load *l*at a node of the microgrid consists of several load types [37,38], depending on their end-use and are denoted by *ty*. These load types include equipment and devices that share similar power factors, harmonic content and flexibility; namely HVAC, domestic hot water (DHW), lights, house appliances and motor drives. The proportion of each load type in the aggregate total load is given by parameter $\eta_{l,ty}^{\text{type,load}}$. Load constraints are given by (2) below:

$$p_{l,ty,t}^{\text{load,min}} = P_{l,t}^{\text{load}}\, \eta_{l,ty}^{\text{type,load}}\, \eta_{ty}^{\text{min,load}}\, \xi_{l,ty,t}^{\text{on,load}} \quad \forall\, l,\, ty,\, t \tag{2a}$$

$$p_{l,ty,t}^{\text{load,max}} = P_{l,t}^{\text{load}}\, \eta_{l,ty}^{\text{type,load}}\, \xi_{l,ty,t}^{\text{on,load}} \quad \forall\, l,\, ty,\, t \tag{2b}$$

$$p_{l,ty,t}^{\text{load,min}} \leqslant p_{l,ty,t}^{\text{load}} \leqslant p_{l,ty,t}^{\text{load,max}} \quad \forall\, l,\, ty,\, t \tag{2c}$$

$$q_{l,ty,t}^{\text{load}} = p_{l,ty,t}^{\text{load}}\, \frac{\sqrt{1-(PF_{ty}^{\text{load}})^2}}{PF_{ty}^{\text{load}}} \quad \forall\, l,\, ty,\, t \tag{2d}$$

$$p_{l,t}^{\text{load,tot}} = \sum_{ty} p_{l,ty,t}^{\text{load}} \quad \forall\, l,\, t \tag{2e}$$

$$q_{l,t}^{\text{load,tot}} = \sum_{ty} q_{l,ty,t}^{\text{load}} \quad \forall\, l,\, t \tag{2f}$$

Eqs. (2a)–(2c) define the range within a load of a specific type can deviate, provided that the load status is active. The status of each load is defined based on the binary decision variable $\xi_{l,ty,t}^{\text{on,load}}$. The reactive power that each load consumes is given by Eq. (2d). One may notice that the reactive power of each load depends on its power factor PF_{ty}^{load}, which subsequently relies upon the type of the load. Eqs. (2e) and 2f simply provide an aggregate value of load types for both active and reactive power. In this paper, we assume that all loads have minimum consumption levels once energized to operate. All load specifications are provided in the electronic companion [33].

3.2. DGs

As already mentioned, the DGs consist of the two APS units (connected to node 2, as shown in Fig. 3), the PV unit (connected to node 8), and the WT unit (connected to node 3). In this work, we assume that the two APS units have minimum power output levels once activated. That is due to the small capacity scale of the microgrid and the fact that the DGs' (but also loads') on and off operations could cause substantial discrete changes in the load curve. The DG constraints are given by (3) below:

$$P_{r,t}^{\text{DG,min}}\, \xi_{r,t}^{\text{DG,on}} \leqslant p_{r,t}^{\text{DG}} \leqslant P_{r,t}^{\text{DG,max}}\, \xi_{r,t}^{\text{DG,on}} \quad \forall\, r,\, t \tag{3a}$$

$$q_{r,t}^{\text{DG,gen}},\, q_{r,t}^{\text{DG,abs}} \geqslant P_{r,t}^{\text{DG,min}}\, \frac{\sqrt{1-(PF_r^{\text{load}})^2}}{PF_r^{\text{load}}}\, \xi_{r,t}^{\text{DG,on}} \quad \forall\, r,\, t \tag{3b}$$

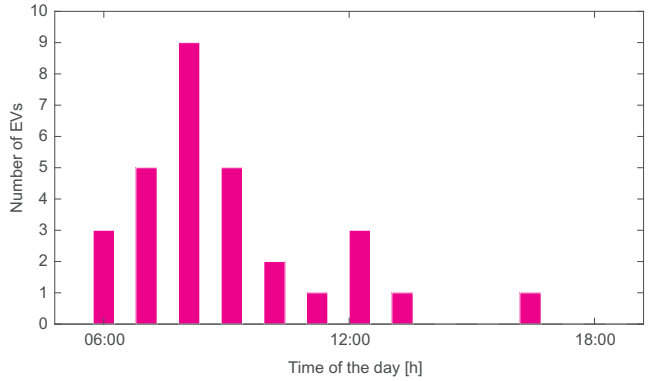

Fig. 2. Arrival time of the EVs.

$$q_{r,t}^{\mathrm{DG,gen}},\ q_{r,t}^{\mathrm{DG,abs}} \leqslant P_{r,t}^{\mathrm{DG,max}} \frac{\sqrt{1-(PF_r^{\mathrm{load}})^2}}{PF_r^{\mathrm{load}}} \xi_{r,t}^{\mathrm{DG,on}} \quad \forall\ r,\ t \tag{3c}$$

$$\xi_{r,t}^{\mathrm{ST}} - \xi_{r,t}^{\mathrm{SD}} = \xi_{r,t}^{\mathrm{DG,on}} - \xi_{r,t-1}^{\mathrm{DG,on}} \quad \forall\ r,\ t \tag{3d}$$

$$\xi_{r,t}^{\mathrm{ST}} + \xi_{r,t}^{\mathrm{SD}} \leqslant 1 \quad \forall\ r,\ t \tag{3e}$$

Eq. (3a) bounds the active power $p_{r,t}^{\mathrm{DG}}$ between the minimum and the maximum power output of each DG. The binary decision variable $\xi_{r,t}^{\mathrm{DG,on}}$ indicates whether the corresponding DG is active or not. Eqs. (3b) and (3c) characterize the generation (absorption) resource reactive power limit constraints. This is to ensure that the power factor of a DG should not exceed its rating. The DGs are generally interfaced with the grid using a fully controllable converter. These converters can absorb or generate reactive power in addition to their active power generation, and they are known as *two-quadrant* converters [39]. Finally, Eq. (3d) and (3e) describe the start-up mechanism of a DG.

3.3. Energy storage

Constraints (4) characterize the ES operation. More specifically, Eq. (4a) and (4b) establish the limitations for the charging ($p_{s,t}^{\mathrm{ES,ch}}$) and discharging ($p_{s,t}^{\mathrm{ES,dis}}$) power of the ES with the assistance of binary variable $\xi_{s,t}^{\mathrm{ES}}$. The state-of-energy (soe) for the ES is expressed by Eq. (4c) and (4d), while Eq. (4e) sets the minimum and the maximum allowed limits for the ES soe. Constraint (4f) ensures that the ES soe at the end of scheduling horizon $t = T$ is at least equal to $SOE_s^{\mathrm{ES,ini}}$. This is important to assure that the model is not biased by being offered a free-of-cost energy source at the beginning of its operation. The implementation of (4f) as an inequality constraint allows the ES to further charge, if such a decision is taken by the optimization algorithm based on the concept of residual energy value. Finally, (4g) expresses the reactive power that can be generated ($q_{s,t}^{\mathrm{ES,gen}}$) or absorbed ($q_{s,t}^{\mathrm{ES,abs}}$) by the ES.

$$0 \leqslant p_{s,t}^{\mathrm{ES,ch}} \leqslant \xi_{s,t}^{\mathrm{ES}}\ P_s^{\mathrm{max,ch}} \quad \forall\ s,\ t \tag{4a}$$

$$0 \leqslant p_{s,t}^{\mathrm{ES,dis}} \leqslant (1-\xi_{s,t}^{\mathrm{ES}})\ P_s^{\mathrm{max,dis}} \quad \forall\ s,\ t \tag{4b}$$

$$soe_{s,t}^{\mathrm{ES}} = SOE_s^{\mathrm{ES,ini}} + \eta_s^{\mathrm{ES,ch}}\ p_{s,t}^{\mathrm{ES,ch}} - \frac{p_{s,t}^{\mathrm{ES,dis}}}{\eta_s^{\mathrm{ES,dis}}} \quad \forall\ s,\ t=1 \tag{4c}$$

$$soe_{s,t}^{\mathrm{ES}} = soe_{s,t-1}^{\mathrm{ES}} + \eta_s^{\mathrm{ES,ch}}\ p_{s,t}^{\mathrm{ES,ch}} - \frac{p_{s,t}^{\mathrm{ES,dis}}}{\eta_s^{\mathrm{ES,dis}}} \quad \forall\ s,\ t>1 \tag{4d}$$

$$SOE_s^{\min} \leqslant soe_{s,t}^{\mathrm{ES}} \leqslant SOE_s^{\max} \quad \forall\ s,\ t \tag{4e}$$

$$soe_{s,T}^{\mathrm{ES}} \geqslant SOE_s^{\mathrm{ES,ini}} \quad \forall\ s \tag{4f}$$

$$0 \leqslant q_{s,t}^{\mathrm{ES,gen}},\ q_{s,t}^{\mathrm{ES,abs}} \leqslant P_s^{\mathrm{ES,max}} \frac{\sqrt{1-(PF_s^{\mathrm{ES}})^2}}{PF_s^{\mathrm{ES}}} \quad \forall\ s,\ t \tag{4g}$$

3.4. Electric vehicles

EVs are considered in this work either as a power supply (when discharging), or as power loads (when charging). We assume that the car fleet consists of 30 EVs and that the EVs are used for work-related trips, while their mobility behaviour remains similar to the one of the conventional vehicles. Usual working hours are considered from 8 am to 6 pm but they are not binding [12].

The EVs' arrival time schedule is fitted in the form of chi-square distribution [40] and its probability density function is given by:

$$f(t_{\mathrm{arr,k}}) = \frac{t_{\mathrm{arr,k}}^{(\upsilon-2)/2}\ e^{-t_{\mathrm{arr,k}}/2}}{2^{\upsilon/2}\ \Gamma(\upsilon/2)} \tag{5}$$

where $\Gamma(\cdot)$ is defined as $\Gamma(\alpha) = \int_0^{\infty} t^{\alpha-1}\ e^{-1}dt$, $\alpha > 0$ with $\upsilon = 4$ degrees of freedom, and $t_{\mathrm{arr,k}}$ is the arrival time for the k-th EV. The chi-square distribution is a good approximation to model the EVs arrival schedule, as most EVs arrive at the parking lots in the morning in accordance with the considered working hours. A deterministic realization of the chi-square distribution described in Eq. (5) is used to obtain the EVs arrival schedule, as illustrated in Fig. 2.

The time during which the EVs remain parked, and thus connected to the microgrid, conforms to the normal distribution with a mean of 8 h and a variance equal to 4 h $\mathrm{N}(8, 2^2)$, assuming that the working period of most people is 8 h. The initial state-of-energy of the EVs batteries conforms to the uniform distribution with a low range of 0.3 and a high range of 0.8 of the battery nominal state-of-energy. Like in the case of EVs arrival schedule, the input data for the parking time of the EVs and their initial battery state-of-energy are obtained from deterministic realizations of their corresponding distributions.

Similarly to the ES modelling constraints, Eq. (6a) and (6b) set a limit on the charging and discharging power of the EVs with the assistance of a binary variable. The available state for an EV at every time-step can be either charging, discharging, or remaining idle. Constraints (6c) and (6d) define the state-of-energy of each EV for the first and the remaining time intervals, respectively. Constraint (6e) limits the EVs' battery minimum and maximum soe to avoid over-charge and over-discharge. In addition, as described earlier, we have added a penalty term in the objective function (1) to prevent unnecessary charging/discharging of the EVs which could lead to potential battery degradation. Finally, Eq. (6f) sets the minimum soe for each EV upon its departure time. The technical details and characteristics of the used EV model (Nissan Leaf) are provided in the electronic companion [33].

$$0 \leqslant p_{k,t}^{\mathrm{EV,ch}} \leqslant \xi_{k,t}^{\mathrm{EV}}\ P^{\mathrm{EV,max,ch}} \quad \forall\ k,\ t \in [T_k^{\mathrm{arr}},\ T_k^{\mathrm{dep}}] \tag{6a}$$

$$0 \leqslant p_{k,t}^{\mathrm{EV,dis}} \leqslant (1-\xi_{k,t}^{\mathrm{EV}})\ P^{\mathrm{EV,max,dis}} \quad \forall\ k,\ t \in [T_k^{\mathrm{arr}},\ T_k^{\mathrm{dep}}] \tag{6b}$$

$$soe_{k,t}^{\mathrm{EV}} = SOE_k^{\mathrm{EV,ini}} + \eta^{\mathrm{EV,ch}}\ p_{k,t}^{\mathrm{EV,ch}} - \frac{p_{k,t}^{\mathrm{EV,dis}}}{\eta^{\mathrm{EV,dis}}} \quad \forall\ k,\ t = T_k^{\mathrm{arr}} \tag{6c}$$

$$soe_{k,t}^{\mathrm{EV}} = soe_{k,t-1}^{\mathrm{EV}} + \eta^{\mathrm{EV,ch}}\ p_{k,t}^{\mathrm{EV,ch}} - \frac{p_{k,t}^{\mathrm{EV,dis}}}{\eta^{\mathrm{EV,dis}}} \quad \forall\ k,\ t \in (T_k^{\mathrm{arr}},\ T_k^{\mathrm{dep}}] \tag{6d}$$

$$SOE^{\mathrm{EV,min}} \leqslant soe_{k,t}^{\mathrm{EV}} \leqslant SOE^{\mathrm{EV,max}} \quad \forall\ k,\ t \in [T_k^{\mathrm{arr}},\ T_k^{\mathrm{dep}}] \tag{6e}$$

$$soe_{k,t}^{\mathrm{EV}} \geqslant SOE_k^{\mathrm{EV,dep}} \quad \forall\ k,\ t = T_k^{\mathrm{dep}} \tag{6f}$$

3.5. Power balance and grid constraints

The active and reactive power balance equations for the whole system are defined in Eq. (7a) and (7b), respectively. More specifically,

the power that is needed to meet the total load demand, the total ES and EVs charge requirements plus the power injected to the grid (if any) and the active losses, must be equal to the power that is generated from the discharge of the ES and the EVs, the power produced by the DGs plus the power drawn from the grid for every time interval t. The reactive power balance constraint (7b) is formulated in a similar way.

$$\sum_{l,ty} p_{l,ty,t}^{\text{load}} + \sum_{s} p_{s,t}^{\text{ES,ch}} + \sum_{k} p_{k,t}^{\text{EV,ch}} + p_t^{\text{grid,out}} + P_t^{\text{loss}} = \sum_{s} p_{s,t}^{\text{ES,dis}} + \sum_{k} p_{k,t}^{\text{EV,dis}} + \sum_{r} p_{r,t}^{\text{DG}} + p_t^{\text{grid,in}} \quad \forall\, t \tag{7a}$$

$$\sum_{l,ty} q_{l,ty,t}^{\text{load}} + \sum_{s} q_{s,t}^{\text{ES,abs}} + \sum_{r} q_{r,t}^{\text{DG,abs}} + q_t^{\text{grid,out}} + Q_t^{\text{loss}} + Q_t^{\text{grid,exch}} = \sum_{s} q_{s,t}^{\text{ES,gen}} + \sum_{r} q_{r,t}^{\text{DG,gen}} + q_t^{\text{grid,in}} \quad \forall\, t \tag{7b}$$

The grid interface constraints realize the logic of power exchange and they are described by (8) below:

$$p_t^{\text{grid,in}} \leqslant \xi_t^{\text{grid}}\, P^{\text{max,grid}} \quad \forall\, t \tag{8a}$$

$$p_t^{\text{grid,out}} \leqslant (1 - \xi_t^{\text{grid}}) P^{\text{max,grid}} \quad \forall\, t \tag{8b}$$

If the EMS needs to draw power from the grid, power is not allowed to be injected into the grid at the same time and vice versa. The limitations in power exchange are imposed by parameter $P^{\text{max,grid}}$ with the assistance of binary variable ξ_t^{grid}.

3.6. Microgrid and DSO interaction framework

This section describes the mechanism used by the EMS of the microgrid to evaluate the power exchanges signals with the DSO. The key needs that could be fulfilled in the distribution system by flexibility services include among others response to unexpected overloading, support in case of voltage violations (power quality), etc [3]. Many DER units are able to alter their generation/consumption pattern with a relatively limited impact on their primary energy service. In reality, the microgrids that could offer DERs flexibility, would be represented by a new commercial player, the Aggregator. This entity would aggregate and mobilize flexibility of DERs and sell it to the highest possible bidder with contract. In case that the DSO is the recipient of the flexibility service, the Aggregator should pay its affiliated microgrids that provide the DERs flexibility from the payment it receives from the DSO. In this sense, the interaction mechanism described in (9) would take place between the microgrid and the Aggregator with DSO being the end-customer.

There are many types of flexibility to support the above needs: handling predictable peak loads in advance or on an event basis, power reserves activated upon request to ensure that the DSO specified capacity limits are not violated on an emergency or planned schedule basis, etc. The interaction mechanism we describe in this paper, being part of a tool that would be mainly used for DA simulations, focuses on evaluating planned (and thus expected) power exchanges with the DSO. One should also note that the development of a more general concept for dealing with distribution-level flexibility services (possibly even through a market clearing auction mechanism) is out of scope of this paper. The interaction framework we develop as part of the general EMS algorithm, aims mainly at investigating the effects of meeting such demands on the power quality of the local microgrid.

Constraints (9a)–(9d) enforce the total power injected to the grid ($p_t^{\text{grid,out}}$), or requested from it ($p_t^{\text{grid,in}}$), to be modified depending on the power alteration requests ($L_t^{\text{sup}\uparrow}$, $L_t^{\text{sup}\downarrow}$, $L_t^{\text{dem}\uparrow}$, $L_t^{\text{dem}\downarrow}$). The requests are valid only if the corresponding auxiliary variables ($\xi_t^{\text{sup}\uparrow}$, $\xi_t^{\text{sup}\downarrow}$, $\xi_t^{\text{dem}\uparrow}$, $\xi_t^{\text{dem}\downarrow}$) obtain non-zero values. The terms $P_t^{\text{grid,out}}$, $P_t^{\text{grid,in}}$ are parameters corresponding to the total power the microgrid would inject to the grid or draw from it, respectively, in normal operation without the DSO signals for power alteration. Finally, the net power alteration based on which the reward is calculated, is expressed by the continuous variables $z_t^{\text{sup}\uparrow}$, $z_t^{\text{sup}\downarrow}$, $z_t^{\text{dem}\uparrow}$, $z_t^{\text{dem}\downarrow}$. Constraints (9e)-(9l) describe their necessary limitations and bounds.

$$p_t^{\text{grid,out}} \geqslant (P_t^{\text{grid,out}} + L_t^{\text{sup}\uparrow})\xi_t^{\text{sup}\uparrow} \quad \forall\, t \tag{9a}$$

$$p_t^{\text{grid,out}} \leqslant (P_t^{\text{grid,out}} - L_t^{\text{sup}\downarrow})\xi_t^{\text{sup}\downarrow} + P^{\text{max,grid}}\,(1 - \xi_t^{\text{sup}\downarrow}) \quad \forall\, t \tag{9b}$$

$$p_t^{\text{grid,in}} \geqslant (P_t^{\text{grid,in}} + L_t^{\text{dem}\uparrow})\xi_t^{\text{dem}\uparrow} \quad \forall\, t \tag{9c}$$

$$p_t^{\text{grid,in}} \leqslant (P_t^{\text{grid,in}} - L_t^{\text{dem}\downarrow})\xi_t^{\text{dem}\downarrow} + P^{\text{max,grid}}\,(1 - \xi_t^{\text{dem}\downarrow}) \quad \forall\, t \tag{9d}$$

$$z_t^{\text{sup}\uparrow} \leqslant \xi_t^{\text{sup}\uparrow}\, P^{\text{max,grid}} \quad \forall\, t \tag{9e}$$

$$z_t^{\text{sup}\uparrow} \leqslant L_t^{\text{sup}\uparrow} \quad \forall\, t \tag{9f}$$

$$z_t^{\text{sup}\downarrow} \leqslant \xi_t^{\text{sup}\downarrow}\, P^{\text{max,grid}} \quad \forall\, t \tag{9g}$$

$$z_t^{\text{sup}\downarrow} \leqslant L_t^{\text{sup}\downarrow} \quad \forall\, t \tag{9h}$$

$$z_t^{\text{dem}\uparrow} \leqslant \xi_t^{\text{dem}\uparrow}\, P^{\text{max,grid}} \quad \forall\, t \tag{9i}$$

$$z_t^{\text{dem}\uparrow} \leqslant L_t^{\text{dem}\uparrow} \quad \forall\, t \tag{9j}$$

$$z_t^{\text{dem}\downarrow} \leqslant \xi_t^{\text{dem}\downarrow}\, P^{\text{max,grid}} \quad \forall\, t \tag{9k}$$

$$z_t^{\text{dem}\downarrow} \leqslant L_t^{\text{dem}\downarrow} \quad \forall\, t \tag{9l}$$

The operation of the power exchange interaction framework with the DSO (or any other that would function as an aggregator to collect the bids from all microgrids) is described in Algorithm 1.

Algorithm 1
Power exchange framework
Data: all optim. inputs and contraints, DSO power requests and financial rewards
Result: decide whether to accept or not the DSO request
initialization;
run optim. and calculate the daily total cost (TC) without DSO requests ;
while $t \leq 24$ **do**
  read the DSO power alteration requests $L_t^{\text{sup}\uparrow}, L_t^{\text{sup}\downarrow}, L_t^{\text{dem}\uparrow}, L_t^{\text{dem}\downarrow}$ and rewards $R_t^{\text{sup}\uparrow}, R_t^{\text{sup}\downarrow}, R_t^{\text{dem}\uparrow}, R_t^{\text{dem}\downarrow}$;
  calculate the updated TC_{DSO} ;
  if $\text{TC}_{\text{DSO}} > \text{TC}$ **then**
    update all necessary related optim. variables to meet DSO request ;
  else
    DSO power requests are not met;
  end
end

4. Power quality framework

In this section, we describe the operation of the power quality improvement iterative algorithm. According to [41], the electric power quality *is a term that refers to maintaining the near sinusoidal waveform of power distribution bus voltages and currents at rated magnitude and frequency*. The concept of power quality includes a variety of different issues. In this work though, we focus only on larger time scale issues (time interval of one hour), such as voltage variations (under-voltage/over-voltage), harmonic distortions, and voltage phase unbalance.

4.1. Voltage variation

The voltage magnitude at a bus can deviate from its rated value. These deviations are often tolerated for small percentages but if they cross certain limits, they are considered as disturbances. These phenomena are mainly caused by an abnormal flow of reactive power in high voltage lines. But at distribution level where microgrids operate, the reactance on resistance ratio (X/R) of a line is lower. Hence, a rise of the active power flow can also affect the voltage. According to [42], the voltage variations in a microgrid should be within ± 5% of the nominal value.

As shown in the short line model between two buses in the electronic companion [33], the voltage drop is highly dependent on the reactive power flow for inductive lines. However, in lines with low X/R ratio, both active and reactive power have an impact on the voltage drop and the phase angle δ between the two buses. Based on this rationale, we define in (10a) the continuous variable $\alpha_{l,t}^{\Delta V}$ which expresses the total active-reactive power relationship of all loads in the microgrid. Eqs. (10b)–(10c) are triggered at every iteration when the amplitude of the voltage is below 95% of its rated value (i.e., $\Delta V \geqslant 0.05$ pu), at every load bus l and time interval t. Parameter $\alpha_{l,t}^{\Delta V,\text{lim}}$ sets the new upper bound for variable $\alpha_{l,t}^{\Delta V}$ at every iteration. The rate of change of this upper bound is set with the help of sensitivity parameter $\lambda_{\Delta V}$. Higher values of $\lambda_{\Delta V}$ result in a steeper decrease of $\alpha_{l,t}^{\Delta V,\text{lim}}$ after each iteration, which consequently causes greater alteration to the loads by the EMS. On the other hand, lower values of $\lambda_{\Delta V}$ would require more iterations for the algorithm to converge (namely to restore power quality indices to acceptable limits).

$$\alpha_{l,t}^{\Delta V}|_{it=i} = p_{l,t}^{\text{load,tot}}|_{it=i} + \left(\frac{X}{R}\right)_l q_{l,t}^{\text{load,tot}}|_{it=i} \quad \forall\, l,\, t \tag{10a}$$

$$\alpha_{l,t}^{\Delta V}|_{it=i+1} \leqslant \alpha_{l,t}^{\Delta V,\text{lim}}|_{it=i+1} \quad \forall\, l,\, t \tag{10b}$$

$$\alpha_{l,t}^{\Delta V,\text{lim}}|_{it=i+1} = \alpha_{l,t}^{\Delta V}|_{it=i}(1 - \lambda_{\Delta V}\ \Delta V_t)|_{it=i} \quad \forall\, l,\, t \tag{10c}$$

4.2. Harmonic distortion

It is known that harmonic distortion in grid voltage leads to non-sinusoidal waveforms. The increased penetration of non-linear power electronic devices along with an increase of sensitive loads have resulted in various concerns over safety and proper operation of electronic equipment. Harmonics are also known to increase the total losses in the system [43]. Higher harmonics can be relatively easily filtered by active/passive filters, or reduced by using appropriate modulation schemes in the command of the power electronics switches. However, lower harmonics (3rd, 5th, 7th, 11th, etc.) are more difficult to filter without reducing at the same time, the signal at base frequency. Harmonic cancellation techniques exist to tackle this problem, but they are not usually cost-effective and they are also technically challenging to implement [44].

Two important measures are defined to identify the extent of harmonic distortion and cope with it. First, the total harmonic distortion (THD) as the percentage of the root mean square (RMS) of the harmonic frequency components against the fundamental frequency component for voltage and current, as presented in (11), respectively:

$$V^{\text{THD}} = \frac{\sqrt{V_2^2 + V_3^2 + \ldots i + V_h^2}}{V_1} \tag{11a}$$

$$I^{\text{THD}} = \frac{\sqrt{I_2^2 + I_3^2 + \ldots i + I_h^2}}{I_1} \tag{11b}$$

where V_h and I_h represent the RMS values of various order harmonics in voltage and current.

According to [45], the limits in low voltage microgrids ($V \leqslant 1$ kV) should not surpass 4% for individual harmonics and 2% for THD at PCC. However, the THD limitation of 2% is practically very challenging and difficult to achieve in microgrids. Thus, the THD limit applicable to higher voltage levels (5%) is preferred [46]. Moreover, in this study we consider current THD for each type of load as a known factor, while we treat the voltage THD originating from current harmonics as a power quality index calculated for each node.

The second measure we introduce to cope with harmonic distortion is presented by the set of equations in (12) below:

$$\alpha_t^{\text{hd}}|_{it=i} = \sum_{l,ty} p_{l,ty,t}^{\text{load}}\Big|_{it=i} I_{ty}^{\text{THD}} \quad \forall\, t \tag{12a}$$

$$\alpha_t^{\text{hd}}|_{it=i+1} \leqslant \alpha_t^{\text{hd,lim}}|_{it=i+1} \quad \forall\, t \tag{12b}$$

$$\alpha_t^{\text{hd,lim}}|_{it=i+1} = \alpha_t^{\text{hd}}|_{it=i}\ (1 - \lambda^{\text{hd}}\ max_l V_{l,t}^{\text{THD}})|_{it=i} \quad \forall\, t \tag{12c}$$

where variable α_t^{hd} represents the total network distortion due to all types of loads. Parameter $\alpha_t^{\text{hd,lim}}$ sets the upper limit for α_t^{hd} in (12b), while its value in each iteration $i$is modified according to sensitivity parameter λ^{hd} and the maximum observed $V_{l,t}^{\text{THD}}$ in all load buses.

4.3. Phase unbalance

According to IEEE, the definition of voltage unbalance is the ratio of the negative-sequence voltage component to the positive-sequence voltage component [47]. In a three-phase system, voltage unbalance takes place when the magnitudes of phase or line voltages are different and the phase angles differ from the balanced conditions, or both [48]. Voltage unbalance is mainly caused when single-phase loads are not evenly distributed across all three phases, and it is often evaluated with the Voltage Unbalance Factor (VUF).

Phase balance constraints (13) ensure that the active power scheduled among the three phases should be within close proximity. At first, variable $\alpha_t^{\text{unb,Ph}(\cdot)}$ in Eqs. (13a)–(13c) is used as a metric for load distribution among all phases. Parameters PhA_l^{dist}, PhB_l^{dist}, and PhC_l^{dist} represent the allocation factors of load $l$to phases A, B, and Cin percentages, respectively. If VUF exceeds 3% [42] in any of load buses $l$at time t, Eqs. (13d)-(13e) are applied. More specifically, a process is initiated which in each iteration $i$modifies variable $\alpha_t^{\text{unb,Ph}(\cdot)}$, so as the VUF factor converges to acceptable levels below 3%. For the convergence to be achieved, in each iteration $i$parameter $\alpha_t^{\text{unb,lim}}$ sets a new upper limit (lower than the limit of the previous iteration) for variable $\alpha_t^{\text{unb,Ph}(\cdot)}$. The rate of change for parameter $\alpha_t^{\text{unb,lim}}$ is decided selecting at each iteration the highest previous value of $\alpha_t^{\text{unb,Ph}(\cdot)}$ and the load bus $l$with the largest VUF. Moreover, this rate can be accelerated or decelerated by adjusting the value of parameter λ^{unb}.

$$\alpha_t^{\text{unb,AB}}|_{it=i} = \left|\sum_l p_{l,t}^{\text{load,tot}}\ (PhA_l^{\text{dist}} - PhB_l^{\text{dist}})\right| \quad \forall\, t \tag{13a}$$

$$\alpha_t^{\text{unb,BC}}|_{it=i} = \left|\sum_l p_{l,t}^{\text{load,tot}}\ (PhB_l^{\text{dist}} - PhC_l^{\text{dist}})\right| \quad \forall\, t \tag{13b}$$

$$\alpha_t^{\text{unb,CA}}|_{it=i} = \left|\sum_l p_{l,t}^{\text{load,tot}}\ (PhC_l^{\text{dist}} - PhA_l^{\text{dist}})\right| \quad \forall\, t \tag{13c}$$

$$\alpha_t^{\text{unb,Ph}(\cdot)}|_{it=i+1} \leqslant \alpha_t^{\text{unb,lim}}|_{it=i+1} \quad \forall\, t,\, Ph \in \{\text{AB, BC, CA}\} \tag{13d}$$

$$\alpha_t^{\text{unb,lim}}|_{it=i+1} = \max_{\text{Ph}(\cdot)}\alpha_t^{\text{unb,Ph}(\cdot)}|_{it=i}\ (1 - \lambda^{\text{unb}}\ \max_l \text{VUF}_{l,t})|_{it=i}$$
$$\forall\ t,\ \text{Ph} \in \{\text{AB, BC, CA}\} \tag{13e}$$

5. Results and discussion

The case studies in this section demonstrate the effectiveness of the proposed energy management system in both achieving the economic objectives in scheduling microgrid's operation and in managing power quality issues.

Algorithm 2 shows the iterative power quality improvement procedure. The optimal energy schedule solution is obtained at first from GAMS without any power quality check. Afterwards, the initial energy schedules on both loads and DERs are evaluated for voltage variation, harmonic distortion, and phase unbalance using OpenDSS. If any violations against the power quality standards occur, then the energy scheduling solution is solved again with constraints (10)-(13) enforced.

The iteration continues until all power quality indices are controlled under requirement levels.

Algorithm 2
Iterative power quality improvement.
Data: the 24h energy sceduling vectors for DERs and loads, power quality limits
Result: power quality improvement
initialization;
it = i;
run the optimization for energy scheduling;
run the power and harmincs loadflow;
calculate $\Delta V, V^{\text{THD}}, VUF$;
if $\Delta V > 0.5$ pu *or* $V^{\text{THD}} > 5\%$ *or* $VUF > 3\%$ **then**
  calulate $\alpha_{t,t}^{\Delta V}, \alpha_t^{\text{hd}}, \alpha_t^{\text{unb,Ph(·)}}$;
  update loads constraints to the new limits ;
  it = i + 1;
  GOTO run the optimization for energy scheduling;
else
  all power quality indices are within standards;
end

In the rest of this section, we first present the microgrid model which has been used across the case studies. We test the EMS and the power quality framework under several demand-response situations and power alteration scenarios. The results are evaluated under both financial and physical system terms (power quality).

As already mentioned in Section 2, the proposed integrated tool performs the simulations using three different software programs: GAMS and CPLEX solver for the EMS, OpenDSS for power and harmonics load flow, and MATLAB for power quality check, scripts handling and results visualization. All simulations were run on an Intel Core i7-5500U CPU @2.4 GHz with 16 GB memory. The execution time for the EMS simulation was 2.86 s. Scripts execution in OpenDSS required 3.78 s. Even in the cases where the iterative power quality improvement forced the continuous sequential execution of the EMS and the power quality framework until all power quality indices were restored to acceptable levels (a maximum number of 3 iterations was needed), the total required elapsed time was less than 30 s.

5.1. The microgrid model

The microgrid model used in this paper is illustrated in Fig. 3. As shown in Fig. 3, the microgrid is connected to the 11.2 kV voltage network through the point of common coupling (PCC). The rest of the microgrid consists of step-down transformers (11.2 kV/400 V) and distribution cables that connect to various building breaker panels. Also, the two 250 kVA generators (APS1 and APS2) are connected to the PCC bus of the microgrid. Three additional DERs are added to the model, including a 165 kVA solar generation unit, a 95 kVA wind generation unit (converter's side), and a 80 kWh, 40 kW energy storage system (ES). The EVs connect to the microgrid through node 10, as depicted in Fig. 3. More information regarding the DERs and their operation is provided in the next section, while the detailed specifications for all microgrid's components are available in the electronic companion [33].

The main electric loads in the microgrid include motors, lighting, and plug loads. In this study, a load is defined as an electric end-use entity, monitored and controlled by the EMS, while we assume that each load (Loads 1, 2 and 3 in Fig. 3) represents an aggregate of different load types. The loads can be in either single phase or three phases, distributed along the lines downstream from the distribution transformers. Among others, the following load capacities are included in the microgrid:

- linear loads such as incandescent lights, space heaters, etc.;
- nonlinear loads including power electronic switching such as variable speed drives, electronic equipment (e.g., computers), and switch mode power supplies;
- small size industrial loads (e.g., duty cycle motor drives).

The harmonic spectrums associated with the various types of nonlinear loads (lightning, electronics, etc.) are defined and based on [49–51]. The various load types are also characterized by their flexibility to be deferred or completely shed. The detailed composition of each load is provided in the electronic companion [33].

The value of lost load is as a monetary expression declaring the costs associated with an interruption of electricity supply [52]. The VOLL can be a useful metric for the EMS that allows for the quantification of the additional cost for the system, when a specific load (or a part of a load) is not met. A different VOLL has been assigned to each load type according to its significance [53]. Therefore, a relatively high VOLL has been assigned to sensitive industrial loads, while the VOLL is lower for more flexible loads (e.g., HVAC systems).

5.2. Base case

The Base case study refers to a typical day of operation for the EMS and the microgrid. One should note that under normal operation, the microgrid is not expected to face any physical or power quality issues. The percentages of each load type for the three aggregated loads (Fig. 3) are set to represent a typical mix of loads, i.e, residential, commercial, and industrial. The wind and solar generation data should reflect forecasts. The bidirectional energy flows between the microgrid

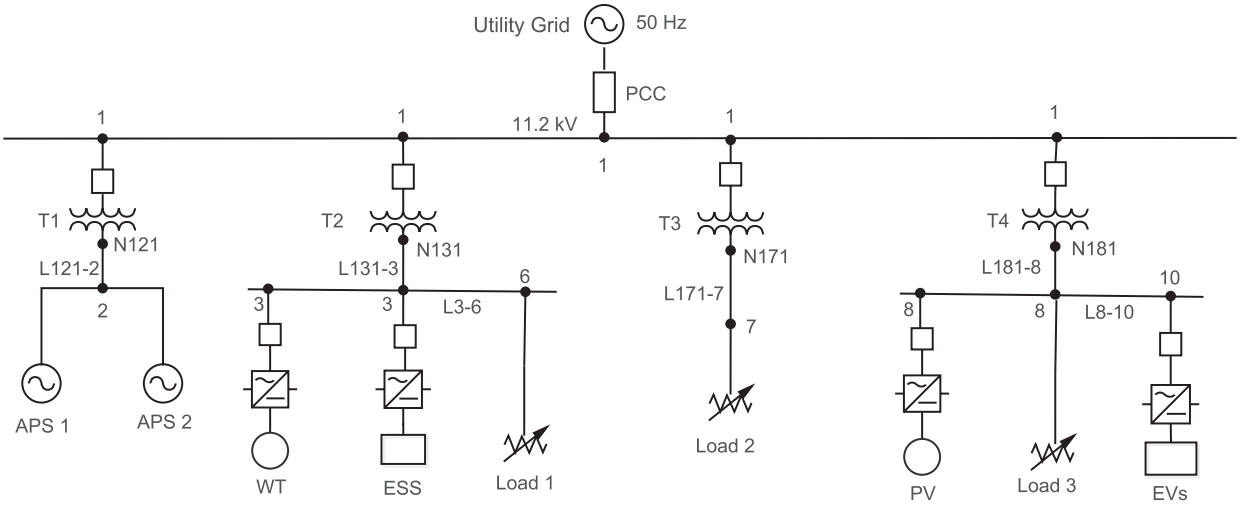

Fig. 3. Microgrid topology.

and the main grid assume the utilization of smart-metering approach. The electricity price rates that have been used in all cases are depicted in Fig. 4. Detailed information regarding the loads composition, renewable forecasts, and DER specifications are provided in the electronic companion [33].

Fig. 5 shows the optimal DERs dispatch and the grid input for a day of normal microgrid operation. The daily total system cost is $**619.34**. There are several observations one might make regarding Fig. 5. First, notice that the grid power input stays positive during the whole day. This implies that the microgrid never encounters a power surplus situation during its daily operation. From 6 am to 8 am, both EVs and ES discharge to aid the microgrid meeting the loads. The main reason for this is that around 7 am, electricity cost reaches its second most expensive value during the day and the EMS tries to mitigate grid power input at that time. A similar pattern is observed during the evening hours (5 pm - 8 pm) where electricity cost reaches its highest value. On the contrary, the optimal time interval to charge the EVs and the ES is in the afternoon (12 pm - 4 pm). One might also notice that the two APS units remain non-operational during all day for Base case. Finally, the charge of the ES at late night hours (10 pm - 12 am) aims at exploiting the concept of ES residual energy.

Fig. 6 shows the voltage evolution (in pu) for all microgrid nodes during the day. One might notice that the voltage levels are within limits (±5% deviation from 1 pu) for all nodes. In addition, we observe no THD or VUF violation, as the highest recorded value does not overpass 1% for either. Therefore, the iterative power quality algorithm is not triggered for the Base case.

5.3. Load variation

In this section, we investigate the reaction of the microgrid in two load variation scenarios. The first one (Case 2a), which is explored in Section 5.3.1, concerns the power exchange framework with the DSO and should be communicated in advance to the interested parties. The second situation (Case 2b in Section 5.3.2) may concern an unexpected load increase/decrease due to, for example, the actualization of an important public event or a grid failure.

5.3.1. DSO interaction

As described in Section 3.6, the flexibility services the DSO might request can vary. In this example, for simplicity and demonstration purposes we have only set two periods during the day, where the power exchange signals are communicated. The time intervals, as well as the power demands with their corresponding rewards are shown in Table 1. In addition, the value of the binary variable for each request shows whether the request has been met or not. During the noon hours, DSO requests concern a supply decrease from the microgrid to the grid, or ideally a demand increase. This is due to the over-voltage, the concurrent injection of active power to the grid coming from PVs, might cause. On the contrary, during the evening hours when the grid mostly encounters the heaviest loads, the DSO requests aim at decreasing the demand and/or, if possible, increasing the supply from the microgrid towards the main grid.

The total system cost for Case 2a is $**364.58**, which represents a 41% cost reduction compared to the Base case. The level of the reward is the most important factor for the EMS to decide whether it meets or not the DSO request. In our example, the maximum reward was set as the double of the highest value electricity price could reach during the day. Moreover, the requested increase/decrease in the load demand corresponds to a 80% change compared to the values $p_t^{\text{grid,in}}$ obtains in Base case for the same time intervals. The requested power levels for $p_t^{\text{grid,out}}$ have been chosen arbitrarily.

Fig. 7 shows the energy scheduling for the DERs and the voltage level in all nodes of the microgrid for Case 2a. One might note that the DERs optimal dispatch has been modified to support the decisions for the DSO interaction. That is, the charge of EVs and ES is shifted earlier in time taking place during the DSO signal for demand increase. We also notice that, in order for the EMS to meet the evening DSO signals for demand decrease/supply increase, the two APS units are activated for the corresponding period. In addition, during this time interval, the microgrid injects power to the grid. As far as power quality is concerned, Fig. 7b indicates that despite the changes in DERs dispatch, voltage levels are still respected in all nodes. The same applies to voltage THD and unbalance where results suggest that no violation of the standards occur.

5.3.2. Microgrid's load alteration

In this case study (Case 2b), we examine microgrid's resilience towards voltage deviations that may occur due to the sudden alteration of one or more loads in the microgrid. More specifically, we consider a 30% increase for Load 1 during a two hours time period (8 pm and 9 pm). It is reminded that Load 1 represents an aggregation of mainly residential loads and it is located in Node 6 of the microgrid.

Fig. 8 illustrates the evolution of voltage levels for all microgrid's nodes. One might notice that the voltage level in Node 6 violates the limit of 0.95 pu during both hours (0.946 pu at 8 pm and 0.943 pu at 9 pm). As a result, constraints (10a)-(10c) are triggered to restore voltage in acceptable limits. As shown in Fig. 8b, after the second iteration, voltage is restored for the first time interval (8 pm), but it is still out of limits for the second one. Finally, after the third iteration (Fig. 8c), voltage levels are settled back to standards for both time intervals. The value of sensitivity parameter $\lambda_{\Delta V}$ for this case has been set to **0.9**.

The activation of the power quality algorithm re-establishes the voltage to acceptable levels but it also affects the total system cost. While in the first iteration the total system cost is $**629.2**, after the third iteration it has increased to $**634.25**. This additional cost is due to the load shed (and thus penalized by the VOLL) by the power quality algorithm during its operation. Finally, voltage THD and unbalance levels are not violated in this case study.

5.4. Harmonic distortion

In the previous case studies, despite the modification of the microgrid energy schedules realized by the EMS to tackle the load variation situations, the THD index remained within the standards limits. In this case study (Case 3), we deliberately modify the harmonic spectrum of the domestic appliances, so as the global THD current of this specific type of load reaches 80%. In addition, the share of the domestic appliances load type for all three aggregated loads of the microgrid is increased by 25%. A scenario like this could, for instance, be realized by the simultaneous operation of electronic devices due to the broadcast of an important sport event.

After the initial energy schedules are obtained from the EMS algorithm solution, they are evaluated by the power quality algorithm for harmonic distortions. Fig. 9 illustrates the voltage THD in microgrid's load nodes. One might notice that the voltage THD requirements are found violated (in our example we impose a stricter limit for THD violation 4% instead of 5%, for demonstration purposes) for Load 1 (located in node 6) during a period of two hours in the evening (8 pm

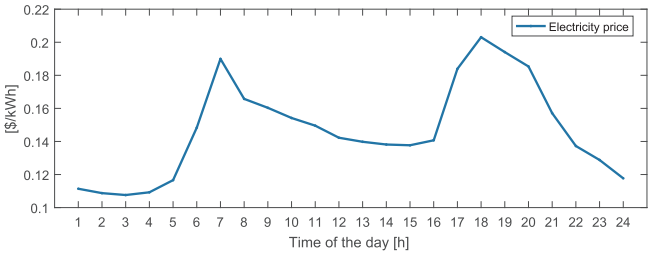

Fig. 4. Electricity price profile during the day.

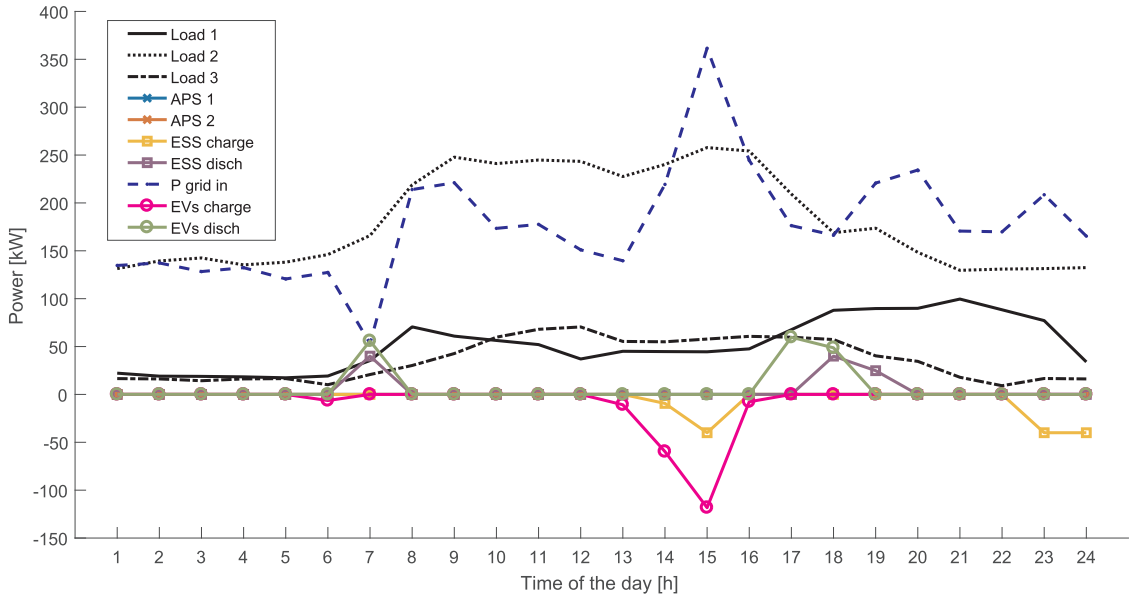

Fig. 5. Optimal DERs dispatch and grid input for Base case.

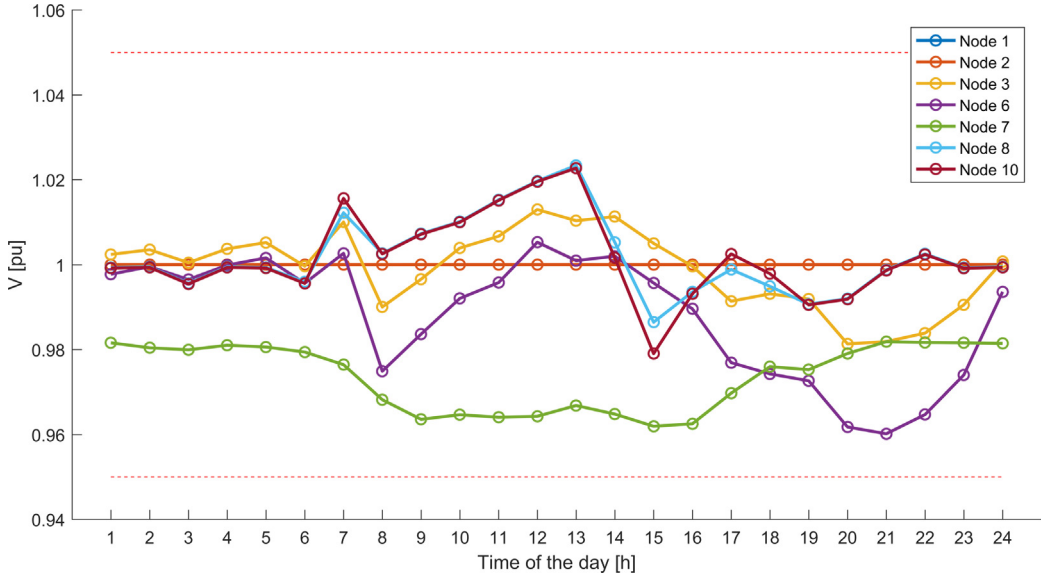

Fig. 6. Voltage in all microgrid's nodes for Base case.

Table 1
The DSO power requests with their corresponding rewards and the auxiliary variables (L is in kWh and R in \$/kWh).

Time	$L_t^{\text{sup}\uparrow}$	$R_t^{\text{sup}\uparrow}$	$\xi_t^{\text{sup}\uparrow}$	$L_t^{\text{sup}\downarrow}$	$R_t^{\text{sup}\downarrow}$	$\xi_t^{\text{sup}\downarrow}$	$L_t^{\text{dem}\uparrow}$	$R_t^{\text{dem}\uparrow}$	$\xi_t^{\text{dem}\uparrow}$	$L_t^{\text{dem}\downarrow}$	$R_t^{\text{dem}\downarrow}$	$\xi_t^{\text{dem}\downarrow}$
12 pm	–	–	–	50	0.3	0	121	0.6	1	–	–	–
1 pm	–	–	–	50	0.3	0	112	0.6	1	–	–	–
7 pm	50	0.6	1	–	–	–	–	–	–	177	0.3	1
8 pm	50	0.6	1	–	–	–	–	–	–	188	0.3	1

and 9 pm). Constraints (12a)-(12c) are activated and two iterations between the EMS and the OpenDSS harmonic solver are required to mitigate the voltage THD violation. In the final energy schedule, the voltage THD meets the limits requirement.

The restoration of voltage THD in acceptable limits causes a slight increase of the total system cost (from \$620.75 to \$624.81). It is important to note that the mitigation of harmonic distortion impact has been achieved mainly by reducing the loads of high harmonic contents. For this case study, the value of sensitivity parameter λ^{hd} has been set to **0.012**. The rest power quality indices (voltage levels and VUF) are not violated in this case study.

5.5. Voltage unbalance

In this case (Case 4), we assume that an unequal distribution of single-phase loads is realized in the microgrid. As a result, the phase distribution for phases B and C of Load 1 is decreased by 60%, while phase A is burdened by an 120% increase. The high unbalance of phase

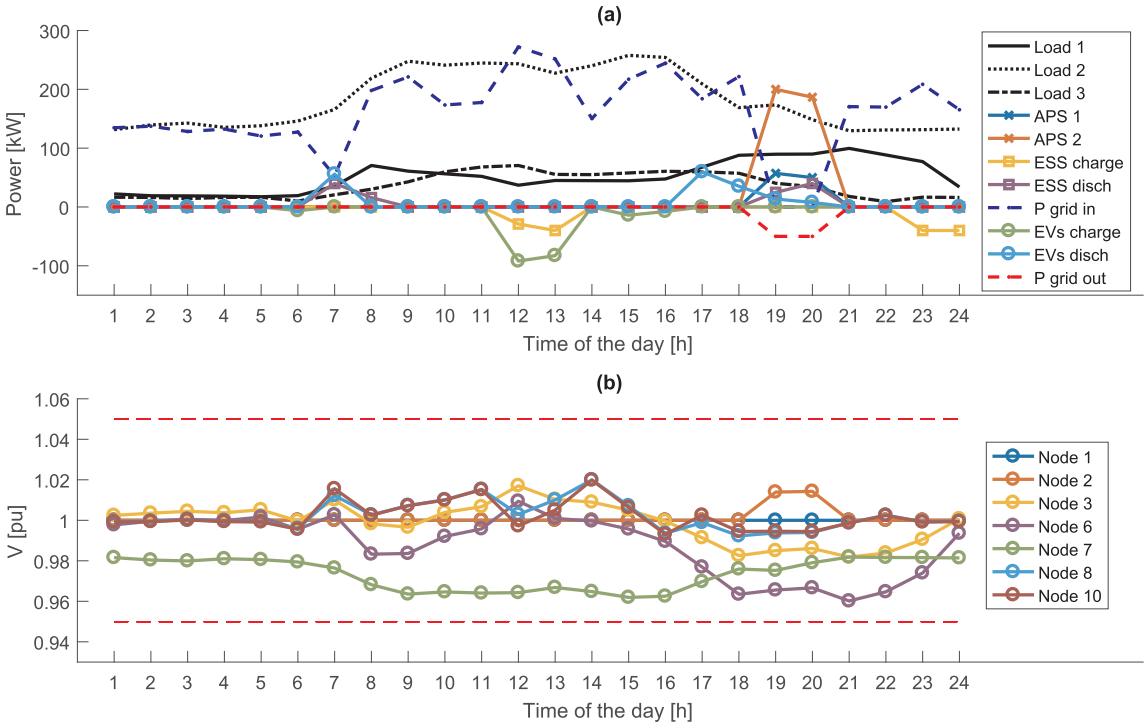

Fig. 7. DERs optimal dispatch (a), and nodes voltage level (b) for Case 2a.

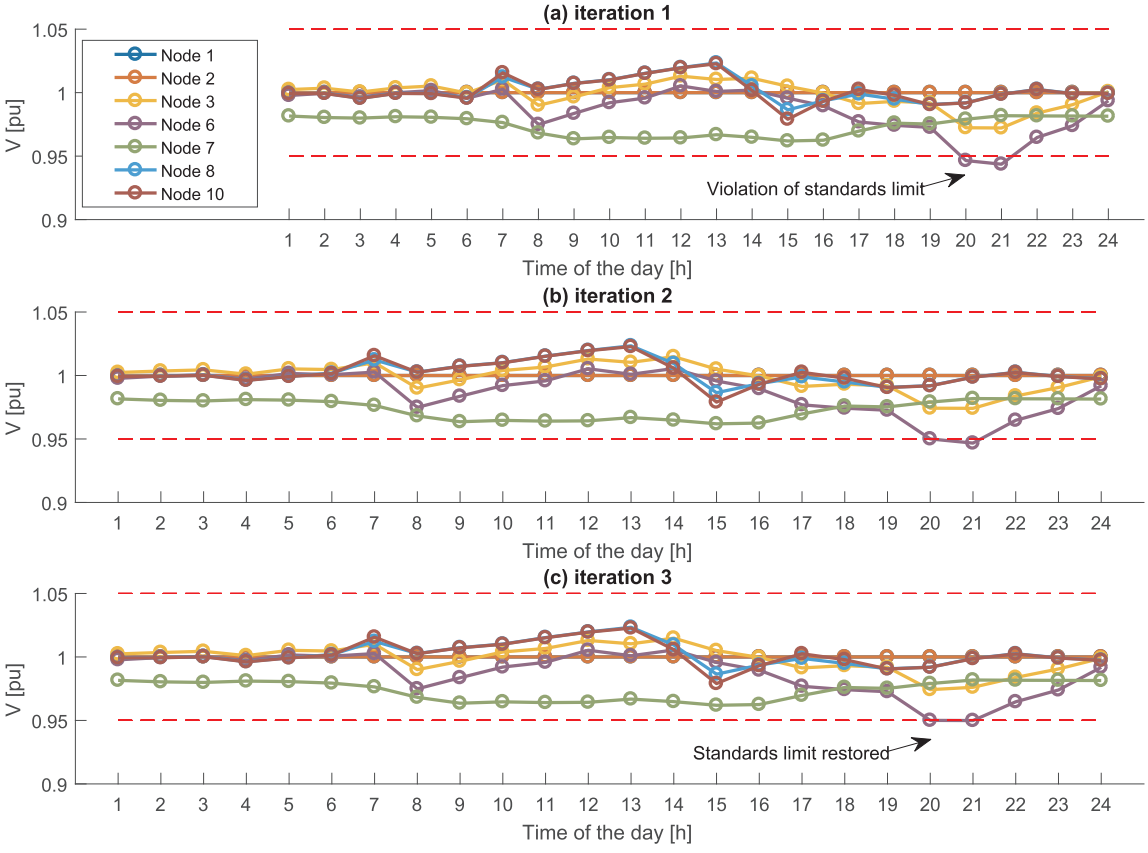

Fig. 8. Voltage evolution during the iterative process in all microgrid's nodes (Case 2b).

A with respect to phase B and C in the residential load (Load 1) is reflected in Fig. 10, where VUF exceeds the limit of 3% at 8 pm and 9 pm. Therefore, constraints (13a)–(13e) are activated and the interaction between the EMS and the power quality algorithm is initiated. After three iterations, the VUF value is mitigated to meet the requirement of 3%. The additional increase in total system's cost due to the activation of the power quality algorithm and the shed load is only **0.75%** (from $619.34 in iteration 1 to $623.96 in iteration 3). For this

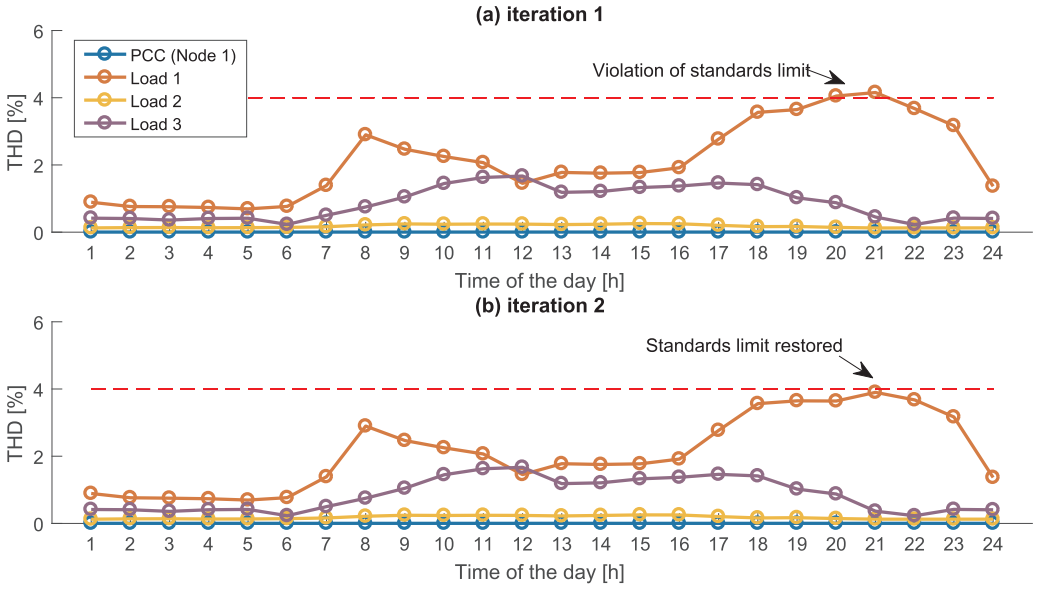

Fig. 9. Voltage THD at load nodes during the iterative process (Case 3).

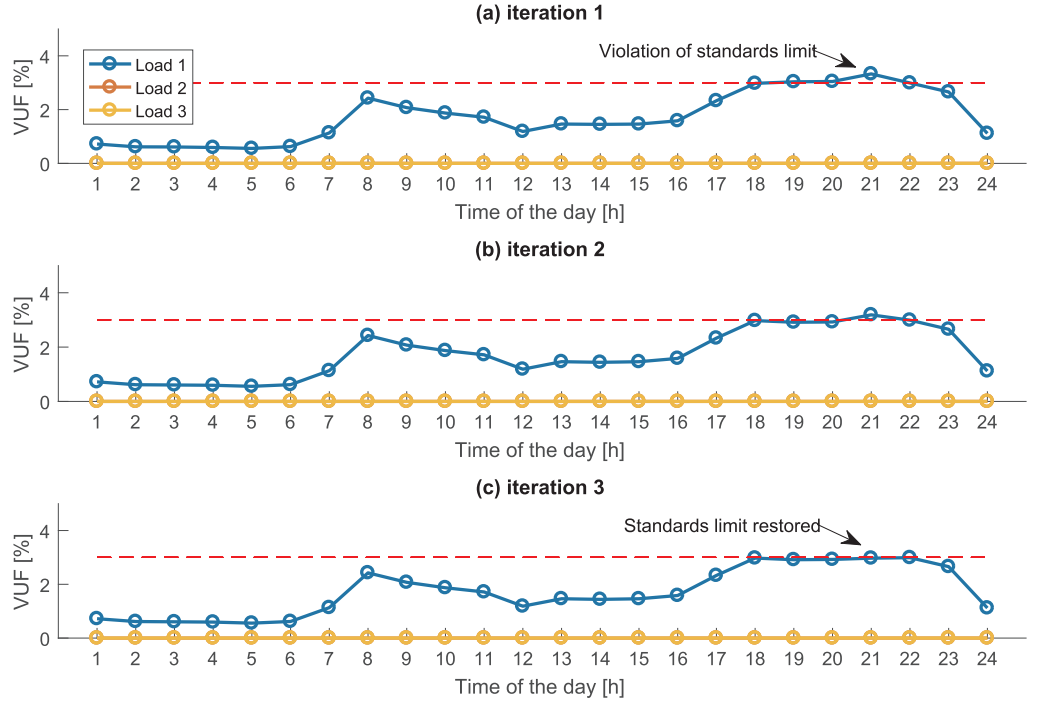

Fig. 10. Voltage unbalance at load nodes during the iterative process (Case 4).

case study, the value of sensitivity parameter λ^{unb} has been set to **0.02**. The remaining power quality indices (voltage levels and voltage THD) are not violated in this case study.

5.6. Off-grid standalone operation

In this scenario (Case 5), grid outage is assumed and the microgrid operates in standalone mode for a period of two hours (from 2 pm to 4 pm). During the energy schedule solution, the grid active power input variable $p_t^{\text{grid,in}}$, as well the grid reactive power input variable $q_t^{\text{grid,in}}$, are forced to be zero throughout the hours of standalone operation. Fig. 11 shows the active and reactive power dispatch of the microgrid's DERs, including the period of standalone operation. During the outage, both active and reactive power requirements of the microgrid loads are covered by modifying the DERs energy scheduling. One of the two APS units is activated to provide both active and reactive power support as illustrated in Fig. 11a and Fig. 11b, respectively. Compared to the Base case (Fig. 5), we notice that the EVs and ESS charge/discharge schedule has been also modified to support the microgrid's off-grid operation. Instead of the single main charge period observed in Base case, the EVs charge in standalone scenario forming two higher lows right before and after the outage interval, while they discharge during the outage period providing an additional source of power. The ES operates in a similar way. We also notice that during the early morning hours (from 1 am until 6 am), the microgrid is able to meet the loads' reactive power requirement internally from its DERs operation.

Fig. 12 presents the voltage levels and the voltage THD at load buses during the 24 h period, including the outage interval. The initial EMS

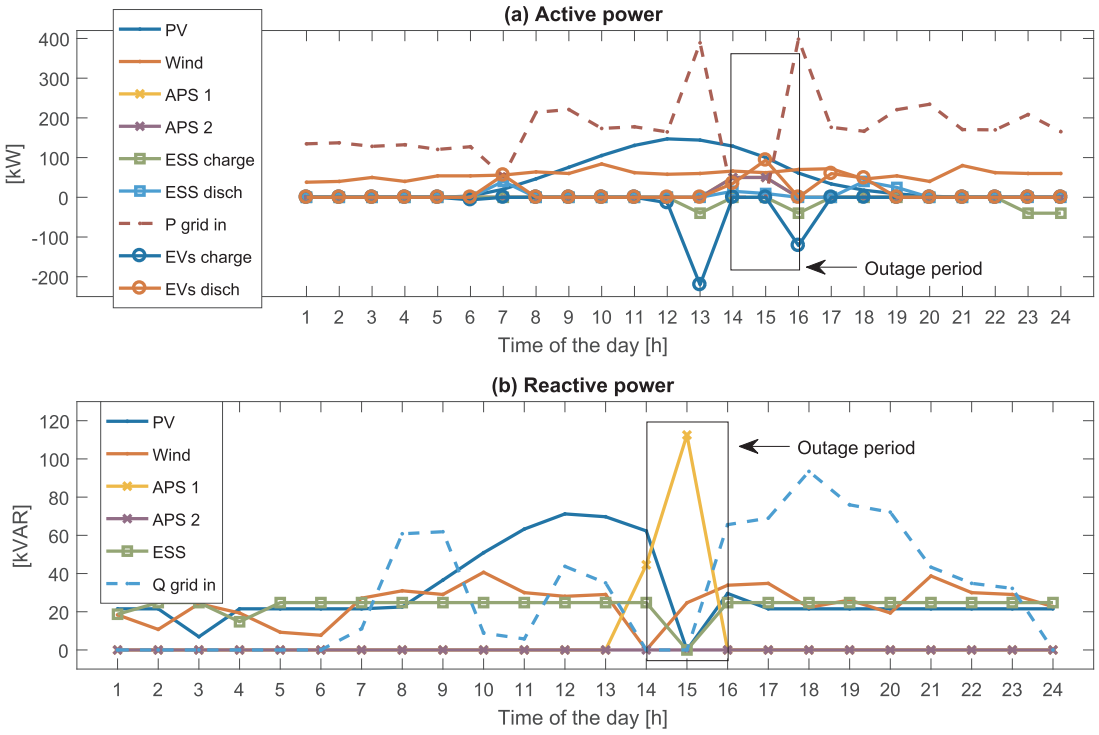

Fig. 11. Active (a), and reactive (b) power for microgrid's standalone operation (Case 5).

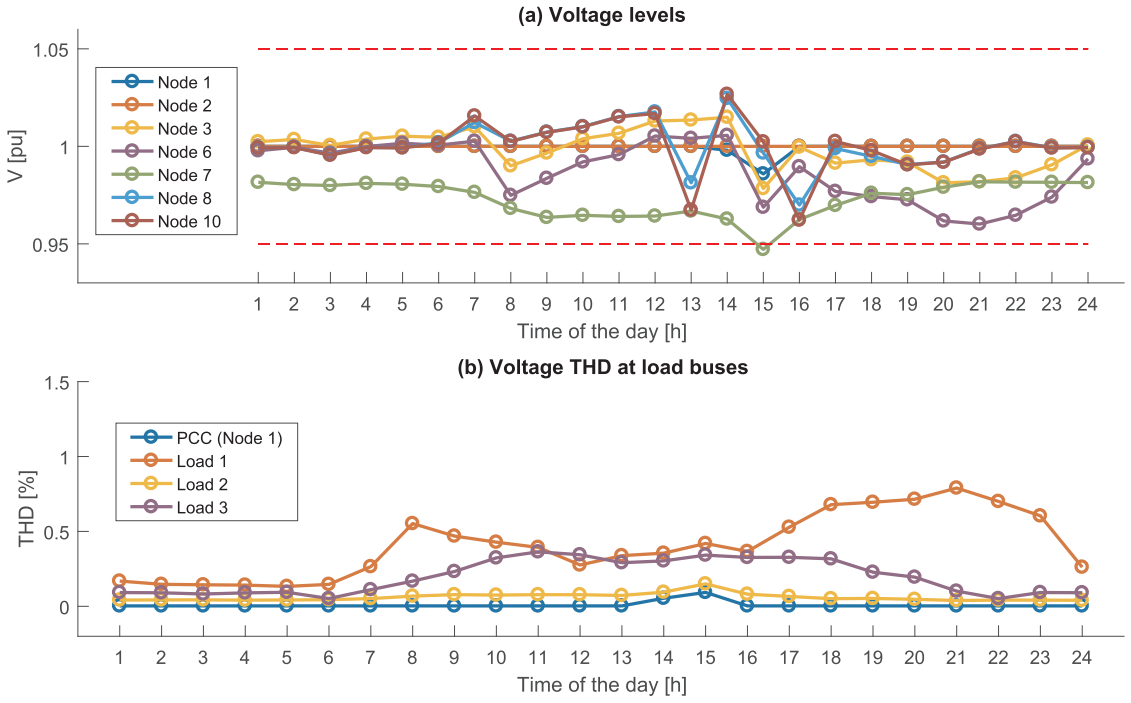

Fig. 12. Voltage levels (a), and voltage THD (b) for microgrid's standalone operation.

scheduling results in a violation of voltage limits during the second hour of the outage event (3 pm) at Node 7, as illustrated in Fig. 12a. Therefore, constraints (10a)–(10c) are activated to restore the voltage value in acceptable levels, as demonstrated in Section 5.3.2. Three iterations of the power quality algorithm are required in total, to fully restore voltage within standards (to avoid repetition, we omit the illustration for the two next iterative steps as this process has been already demonstrated in Section 5.3.2). On the contrary, although a small fluctuation is observed in the voltage THD during the outage period, the THD limits are not violated either in the load buses or the PCC. The total system cost increases from **$666.05** (first iteration) to **$668.51** (third iteration).

6. Conclusion and future work

Energy management and power quality issues are of high importance for the smooth operation of small capacity microgrids such as those serving small to medium size loads. This paper proposes an

integrated tool for the effective mitigation of power quality issues in a microgrid operation through the coordination of a MILP-based energy scheduling algorithm and an iterative power quality improvement algorithm. The EMS attempts to realize minimum total system cost through coordinating the operation schedules of the microgrid's DERs and loads, while the power quality algorithm monitors the system for potential voltage deviations, harmonic distortions, and voltage unbalance during its operation. The presented case studies demonstrate the efficacy of the proposed energy management integrated tool in both achieving the economic objectives in scheduling microgrid's operation and in effectively mitigating its power quality issues. In the majority of the case studies, a maximum number of three iterations is required to restore the power quality requirements to acceptable levels for the considered sensitivity parameters, with a small additional cost for the system. The proposed energy management framework can be implemented in a commercial environment where building automated systems are present, and with DERs and loads managed by device agents on an EMS platform.

Recommendations for future work include the introduction of stochasticity (e.g., for renewable generation, loads, electricity price) in the integrated tool and the investigation of additional case studies. Moreover, as several standards (see for instance EN 50160) dealing with voltage characteristics in statistical or probabilistic terms allow for a short term voltage limit violation (e.g., for no more than 5% over a given operation time), we specifically propose using chance constrained optimization to model this source of uncertainty.

Declaration of Competing Interest

None.

Acknowledgements

The authors would like to thank the two anonymous reviewers for their valuable comments and remarks. This research was funded by EC under the FP7 RE-SIZED 621408 (Research Excellence for Solutions and Implementation of Net-Zero Energy City Districts) project.

Appendix A. Supplementary material

Supplementary data associated with this article can be found, in the online version, at https://doi.org/10.1016/j.apenergy.2019.114314.

References

[1] Katiraei F, Iravani R, Hatziargyriou N, Dimeas A. Microgrids management. IEEE Power Energ Mag 2008;6(3):54–65. https://doi.org/10.1109/MPE.2008.918702.
[2] Hatziargyriou N. Microgrid: architectures and control. Wiley; 2013.
[3] Heussen K, Bondy DEM, Hu J, Gehrke O, Hansen LH. A clearinghouse concept for distribution-level flexibility services. In: 2013 4th IEEE/PES innovative smart grid technologies Europe (ISGT EUROPE), p. 1–5. https://doi.org/10.1109/ISGTEurope.2013.6695483.
[4] Zhao B, Wang X, Lin D, Calvin MM, Morgan JC, Qin R, et al. Energy management of multiple microgrids based on a system of systems architecture. IEEE Trans Power Syst 2018;33(6):6410–21. https://doi.org/10.1109/TPWRS.2018.2840055.
[5] Salahuddin U, Berthold A. Design and development of industrial microgrids; 2015. <https://library.e.abb.com/public/7c90f8946127403d89fa7887165af392/DEABB%205084%2015%20Design%20and%20development%20of%20microgrids%20White%20paper_rev4.pdf>.
[6] Bashir AA, Pourakbari-Kasmaei M, Contreras J, Lehtonen M. A novel energy scheduling framework for reliable and economic operation of islanded and grid-connected microgrids. Electr Power Syst Res 2019;171:85–96. https://doi.org/10.1016/j.epsr.2019.02.010.
[7] Özkan HA. A new real time home power management system. Energy Build 2015;97:56–64. https://doi.org/10.1016/j.enbuild.2015.03.038.
[8] Matallanas E, Castillo-Cagigal M, Gutiérrez A, Monasterio-Huelin F, Caamaño-Martín E, Masa D, et al. Neural network controller for active demand-side management with pv energy in the residential sector. Appl Energy 2012;91(1):90–7. https://doi.org/10.1016/j.apenergy.2011.09.004.
[9] Xue X, Wang S, Sun Y, Xiao F. An interactive building power demand management strategy for facilitating smart grid optimization. Appl Energy 2014;116:297–310. https://doi.org/10.1016/j.apenergy.2013.11.064.
[10] Chen Z, Wu L, Fu Y. Real-time price-based demand response management for residential appliances via stochastic optimization and robust optimization. IEEE Trans Smart Grid 2012;3(4):1822–31. https://doi.org/10.1109/TSG.2012.2212729.
[11] Bendato I, Bonfiglio A, Brignone M, Delfino F, Pampararo F, Procopio R. A real-time energy management system for the integration of economical aspects and system operator requirements: definition and validation. Renew Energy 2017;102:406–16. https://doi.org/10.1016/j.renene.2016.10.061.
[12] Thomas D, Deblecker O, Ioakimidis CS. Optimal operation of an energy management system for a grid-connected smart building considering photovoltaics' uncertainty and stochastic electric vehicles' driving schedule. Appl Energy 2018;210:1188–206. https://doi.org/10.1016/j.apenergy.2017.07.035.
[13] Liu Z, Wu Q, Huang S, Wang L, Shahidehpour M, Xue Y. Optimal day-ahead charging scheduling of electric vehicles through an aggregative game model. IEEE Trans Smart Grid 2017;1. https://doi.org/10.1109/TSG.2017.2682340.
[14] Thomas D, Deblecker O, Ioakimidis CS. Optimal design and techno-economic analysis of an autonomous small isolated microgrid aiming at high res penetration. Energy 2016;116:364–79. https://doi.org/10.1016/j.energy.2016.09.119.
[15] Sousa T, Vale Z, Carvalho JP, Pinto T, Morais H. A hybrid simulated annealing approach to handle energy resource management considering an intensive use of electric vehicles. Energy 2014;67:81–96. https://doi.org/10.1016/j.energy.2014.02.025.
[16] Ioakimidis CS, Thomas D, Rycerski P, Genikomsakis KN. Peak shaving and valley filling of power consumption profile in non-residential buildings using an electric vehicle parking lot. Energy 2018;148:148–58. https://doi.org/10.1016/j.energy.2018.01.128.
[17] Mortaz E, Valenzuela J. Microgrid energy scheduling using storage from electric vehicles. Electr Power Syst Res 2017;143:554–62. https://doi.org/10.1016/j.epsr.2016.10.062.
[18] Sousa T, Morais H, Vale Z, Castro R. A multi-objective optimization of the active and reactive resource scheduling at a distribution level in a smart grid context. Energy 2015;85:236–50. https://doi.org/10.1016/j.energy.2015.03.077.
[19] Zhang D, Evangelisti S, Lettieri P, Papageorgiou LG. Economic and environmental scheduling of smart homes with microgrid: Der operation and electrical tasks. Energy Convers Manage 2016;110:113–24. https://doi.org/10.1016/j.enconman.2015.11.056.
[20] Coelho VN, Coelho IM, Coelho BN, Cohen MW, Reis AJ, Silva SM, et al. Multi-objective energy storage power dispatching using plug-in vehicles in a smart-microgrid. Renew Energy 2016;89:730–42. https://doi.org/10.1016/j.renene.2015.11.084.
[21] Aghajani GR, Shayanfar HA, Shayeghi H. Presenting a multi-objective generation scheduling model for pricing demand response rate in micro-grid energy management. Energy Convers Manage 2015;106:308–21. https://doi.org/10.1016/j.enconman.2015.08.059.
[22] Christo TMd, Perron S, Fardin JF, Simonetti DSL, Alvarez CEd. Demand-side energy management by cooperative combination of plans: a multi-objective method applicable to isolated communities. Appl Energy 2019;240:453–72. https://doi.org/10.1016/j.apenergy.2019.02.011.
[23] Efkarpidis N, Rybel Td, Driesen J. Technical assessment of centralized and localized voltage control strategies in low voltage networks,. Sustain Energy, Grids Networks 2016;8:85–97. https://doi.org/10.1016/j.segan.2016.09.003.
[24] Yazdi F, Hosseinian SH. A novel "smart branch" for power quality improvement in microgrids. Int J Electr Power Energy Syst 2019;110:161–70. https://doi.org/10.1016/j.ijepes.2019.02.026.
[25] Adnan M, Tariq M, Zhou Z, Poor HV. Load flow balancing and transient stability analysis in renewable integrated power grids. Int J Electr Power Energy Syst 2019;104:744–71. https://doi.org/10.1016/j.ijepes.2018.06.037.
[26] Ortega MJ, Hernández JC, García OG. Measurement and assessment of power quality characteristics for photovoltaic systems: harmonics, flicker, unbalance, and slow voltage variations. Electr Power Syst Res 2013;96:23–35. https://doi.org/10.1016/j.epsr.2012.11.003.
[27] Niitsoo J, Taklaja P, Palu I, Klüss J. Power quality issues concerning photovoltaic generation and electrical vehicle loads in distribution grids. Smart Grid Renew Energy 2015;06(06):164–77. https://doi.org/10.4236/sgre.2015.66015.
[28] Elkholy MM, El-Hameed MA, El-Fergany AA. Harmonic analysis of hybrid renewable microgrids comprising optimal design of passive filters and uncertainties. Electr Power Syst Res 2018;163:491–501. https://doi.org/10.1016/j.epsr.2018.07.023.
[29] Khaledian A, Vahidi B, Abedi M. Harmonic distorted load control in a microgrid. J Appl Res Technol 2014;12(4):792–802. https://doi.org/10.1016/S1665-6423(14)70095-1.
[30] GAMS Development Corporation, GAMS. <https://www.gams.com/>.
[31] MathWorks, MATLAB. <https://nl.mathworks.com/products/matlab.html>.
[32] Electric Power Research Institute, OpenDSS. <http://smartgrid.epri.com/SimulationTool.aspx>.
[33] Thomas D, D'Hoop G, Deblecker O, Genikomsakis KN, Ioakimidis CS. Electronic companion - an integrated tool for optimal energy scheduling and power quality improvement of a microgrid under multiple demand response schemes; 2019. https://doi.org/10.5281/zenodo.3298279.
[34] Ioakimidis CS, Oliveira LJ, Genikomsakis KN, Dallas PI. Design, architecture and implementation of a residential energy box management tool in a smartgrid. Energy 2014;75:167–81. https://doi.org/10.1016/j.energy.2014.07.068.
[35] Ding H, Pinson P, Hu Z, Song Y. Optimal offering and operating strategies for wind-storage systems with linear decision rules. IEEE Trans Power Syst 2016;31(6):4755–64. https://doi.org/10.1109/TPWRS.2016.2521177.
[36] Ding H, Pinson P, Hu Z, Song Y. Integrated bidding and operating strategies for wind-storage systems. IEEE Trans Sustain Energy 2016;7(1):163–72. https://doi.

org/10.1109/TSTE.2015.2472576.
[37] United States Energy Information Administration, Annual energy outllok: Aeo2018; 2018.
[38] McKenna E, Thomson M. High-resolution stochastic integrated thermal–electrical domestic demand model. Appl Energy 2016;165:445–61. https://doi.org/10.1016/j.apenergy.2015.12.089.
[39] Turitsyn K, Sulc P, Backhaus S, Chertkov M. Options for control of reactive power by distributed photovoltaic generators. Proc IEEE 2011;99(6):1063–73. https://doi.org/10.1109/JPROC.2011.2116750.
[40] Wang D, Guan X, Wu J, Li P, Zan P, Xu H. Integrated energy exchange scheduling for multimicrogrid system with electric vehicles. IEEE Trans Smart Grid 2016;7(4):1762–74. https://doi.org/10.1109/TSG.2015.2438852.
[41] Chattopadhyay S, Mitra M, Sengupta S. Electric power quality. Netherlands, Dordrecht: Springer; 2011. https://doi.org/10.1007/978-94-007-0635-4.
[42] IEEE, Guide for design, operation, and integration of distributed resource island systems with electric power systems; 2011. https://doi.org/10.1109/IEEESTD.2011.5960751.
[43] Mahdi Share Pasand M. Harmonic aggregation techniques. J Electr Electron Eng 2015;3(5):117. https://doi.org/10.11648/j.jeee.20150305.13.
[44] Mazin HE, Xu W. Harmonic cancellation characteristics of specially connected transformers. Electr Power Syst Res 2009;79(12):1689–97. https://doi.org/10.1016/j.epsr.2009.07.006.
[45] Hoevenaars T, LeDoux K, Colosino M. Interpreting ieee std 519 and meeting its harmonic limits in vfd applications. In: IEEE petroleum and chemical industry technical conference, 15–17 Sept.; 2003. p. 145–50. https://doi.org/10.1109/PCICON.2003.1242609.
[46] Grady WM, Santoso S. Understanding power system hannonics. IEEE Power Eng Rev 2001;21(11):8–11. https://doi.org/10.1109/MPER.2001.961997.
[47] Bollen M. Definitions of voltage unbalance. IEEE Power Eng Rev 2002;22(11):49–50.
[48] IEEE. Definitions of voltage unbalance. Power Eng Rev 2001;21: 49–51. https://doi.org/10.1109/MPER.2001.4311362.
[49] Shakila Priyadharshini AR, Devarajan Nanjundappan, Uma saranya AR, Anitt R. Survey of harmonics in non linear loads; 2012.
[50] Nikum K, Saxena R, Wagh A. Harmonic analysis of residential load based on power quality. In: 2016 IEEE 7th power india international conference (PIICON), p. 1–6. https://doi.org/10.1109/POWERI.2016.8077306.
[51] Majithia CA, Desai AV, Panchal AK. Harmonic analysis of some light sources used for domestic lighting. Light Res Technol 2011;43(3):371–80. https://doi.org/10.1177/1477153510394597.
[52] Schröder T, Kuckshinrichs W. Value of lost load: an efficient economic indicator for power supply security? a literature review. Front Energy Res 2015;3:1378. https://doi.org/10.3389/fenrg.2015.00055.
[53] Pipattanasomporn M, Kuzlu M, Rahman S, Teklu Y. Load profiles of selected major household appliances and their demand response opportunities. IEEE Trans Smart Grid 2014;5(2):742–50. https://doi.org/10.1109/TSG.2013.2268664.